Received 12 October 2020; accepted 26 October 2020. Date of publication 30 October 2020; date of current version 20 November 2020.

Digital Object Identifier 10.1109/OJCOMS.2020.3035118

Constrained Channel Decomposition-Based Hybrid Beamforming for mmWave Massive MIMO Systems

GUILHERME MARTIGNAGO ZILLI (Graduate Student Member, IEEE), AND WEI-PING ZHU (Senior Member, IEEE)

Department of Electrical and Computer Engineering, Concordia University, Montreal, QC H3G 1M8, Canada

CORRESPONDING AUTHOR: G. M. ZILLI (e-mail: guilherme.m.zilli@gmail.com)

This work was supported in part by the Fonds de Recherche du Québec–Nature et Technologies (FRQNT), and in part by the Natural Sciences and Engineering Research Council of Canada (NSERC).

ABSTRACT In this article, we propose a hybrid beamforming design for multiuser mmWave massive MIMO systems. We adopt a two-stage approach for designing the analog and digital beamforming separately. The analog beamforming design is based on a constrained low-rank channel decomposition and aims to simultaneously harvest the array gain and reduce the intra- and inter-user interference. The digital beamforming design is conducted by using the regularized channel diagonalization method, which provides a better trade-off between multiuser interference suppression and transmit diversity, thus attaining a better performance in low-SNR scenarios or when communicating to many users or through many data streams. We validate the effectiveness of the proposed design through numerical simulations, which have shown that our design outperforms several other hybrid beamforming designs in the literature.

INDEX TERMS Constrained low-rank decomposition, hybrid beamforming, multiuser MIMO, millimeter wave, regularized channel diagonalization.

I. INTRODUCTION

THE OVERGROWING demand for high data throughput, the increasing number of connected devices, and the emergence of new services and applications have imposed 5G and beyond-5G (B5G) wireless communication systems a soaring requirement for higher spectral and energy efficiency [1]–[4]. Since the early envisioning of the 5G system, massive MIMO and millimeter waves (mmWave) have been considered as key technologies to achieve these requirements [5], [6]. Likewise, B5G systems will also rely on these technologies, while continuing to move to higher frequencies, such as the terahertz (THz) band [7]. Although mmWave and THz bands are able to provide large continuous unused/underused bandwidths, allowing much higher data rates, these frequencies are severely affected by path loss, penetration loss, and atmospheric attenuation [8], [9]. Therefore, massive MIMO plays an important role in mitigating these adverse propagation effects. Nevertheless, the cost and power consumption of radio-frequency (RF) chains, particularly at high frequencies, and the space occupied by such devices, can forbid massive MIMO systems from using conventional fully-digital beamforming (which requires one RF chain per antenna) [10], [11]. A promising alternative is a hybrid beamforming (HBF) architecture [11]–[15].

HBF combines a high-dimensional analog beamforming, usually comprised of a network of variable phase shifters (PSs), and a low-dimensional digital beamforming, which are connected through a limited number of RF chains (e.g., much smaller than the number of antennas) [10], [11]. This architecture can achieve near-optimal performance, supported by the high array and multiplexing gains of massive MIMO while allowing reduced power consumption and hardware complexity. On the other hand, the coupling between analog and digital beamforming and the constant modulus constraint imposed by the PSs lead to non-linear and non-convex design problems [16].

A. RELATED WORKS

The HBF design for single-user mmWave massive MIMO systems has been addressed in [17]–[21]. In [17], El Ayach *et al.*, demonstrated that HBF design for spectral efficiency maximization can be recast as a sparse approximation problem, which aims to find the HBF that best

approximates the optimal unconstrained beamforming (given by the channel matrix's SVD). To solve this approximation problem, the authors in [17] exploit the structure of the mmWave channel and introduced the Orthogonal Matching Pursuit (OMP) algorithm, which performs an exhaustive search over the array response vector codebook to design the analog beamforming. In [18], the authors solve this approximation problem with an alternating minimization algorithm that iteratively designs the digital and analog precoders, using closed-form solutions and phase-extraction (PE) to ensure the feasibility of the analog precoder. Instead of using approximation methods, the authors in [19] designed the HBF by directly tackling the rate maximization problem. After extracting the contribution of each element of the analog beamforming to the system's rate, they presented an iterative coordinate descent algorithm to successively update each of these elements. In [20], authors presented a simple yet efficient PE-based HBF design, where the analog beamforming is simply obtained by extracting the phases of the unconstrained optimal beamforming, while the baseband beamforming is obtained by the least-squares solution. Most recently in [21], the authors have proposed a constrained-SVD (CSVD)-based joint hybrid precoder and combiner design, in which analog precoders and combiners are, respectively, the "pseudo" right and left constrained singular vectors with constant modulus entries.

The promising results obtained in single-user (SU)-MIMO HBF encouraged researchers to further investigate its use in multiuser (MU)-MIMO systems [22]–[32]. Early works on MU-MIMO HBF design have considered the single data stream transmission for single-antenna [22], [23] and multi-antenna [24]–[27] mobile users. In these works, the analog beamforming is often designed to harvest the array gain by either using equal gain transmission (EGT) [22], performing an exhaustive search over an analog beamforming codebook [24], [25], or extracting the phases of the channel's principal singular vector pair [26], without accounting for the multiuser interference (MUI). A different approach has been taken in [23] and [27], where authors proposed analog beamforming designs to simultaneously maximize each user's equivalent channel gain and mitigate the MUI using Gram-Schmidt-based approaches. The digital precoder, on the other hand, is often designed by the zero-forcing (ZF) method. The ZF precoder allows a complete diagonalization of the effective channel, thus suppressing all inter-user interference. When multi-antenna receivers are considered, however, the complete channel diagonalization at the transmitter using ZF precoder is sub-optimal since the receiver can employ coordinate processing to help to reduce the interference [33]. The alternative is a generalization of the ZF processing for multi-antenna users, known as block diagonalization (BD) [33].

The MU-MIMO HBF design for multiple data stream transmission has been considered in [28]–[32]. In [28], the authors introduced the hybrid BD (Hy-BD) scheme, in which the analog combiner and precoder are designed by using, respectively, exhaustive search over a DFT codebook and EGT, in order to harvest the array gain. The digital precoder and combiner are designed by the BD method over the low-dimensional baseband effective channel. In [29], the authors presented a subspace projection aided BD scheme for fully-digital beamforming design using the angle of departure information and used an iterative matrix decomposition to obtain the hybrid precoder and combiner from the fully-digital solution. Authors in [30] devised a two-stage method, in which first, the analog precoder and combiner are designed aiming to maximize the capacity of effective baseband channel, and then, the digital precoder and combiner are obtained from the traditional BD. In [31], the authors have designed the analog beamforming using an approach similar to [19], and also obtained the digital beamforming from the traditional BD. Finally, the author in [32] introduced the hybrid regularized channel diagonalization (HRCD) that uses exhaustive search over the array response vector codebook for designing the analog combiner, EGT for the analog precoder, and regularized channel diagonalization for the digital precoder and combiner. Note that the analog beamforming design in [22], [24]–[26], [28], [29], [31], and [32] seeks to provide higher baseband effective channel gain, thus increasing the desired signal's power at the receiver, but do not attempt to reduce inter- and intra-user interference. The interference mitigation is performed only at the digital beamforming stage. And although the methods in [23] and [27] can reduce MUI, they are designed for single data stream transmission and therefore, do not account for intra-user interference. Moreover, the methods in [29], [32] rely on the perfect knowledge of the steering vectors of all propagation paths.

B. MAIN CONTRIBUTIONS

In this article, we present a novel joint hybrid precoder and combiner design for multiuser mmWave massive MIMO systems. The major contributions of this article are summarized as follows:

- First, we present a two-stage approach for designing the analog precoder and combiner and their digital counterpart. The analog precoder and combiner are designed to harvest the array gain provided by the massive MIMO system while simultaneously reducing the intra-user and MUI interference. Such a design is formulated as a constrained low-rank channel decomposition problem based on the constant modulus constraint imposed by the PS, resulting in an intractable problem. To make the problem tractable, we propose a successive rank-1 channel decomposition approach to successively compute each analog precoder and combiner vector pair. The rank-1 channel decomposition problem is then solved by using the projected block coordinate descent method.
- The digital precoder and combiner are computed using the regularized channel diagonalization approach [32], aiming to minimize the MUI plus noise. In contrast with

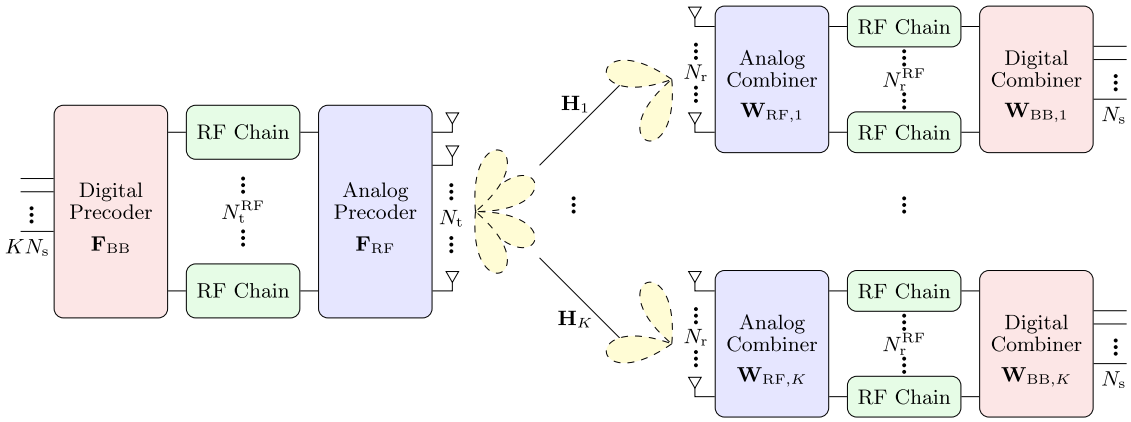

FIGURE 1. System diagram for the downlink of a multiuser massive MIMO system with hybrid beamforming.

the traditional BD method, which only focuses on canceling the MUI, the regularized channel diagonalization trades off MUI suppression for more transmit diversity, thus leading to a better performance in scenarios with low-SNR or high number of users/data streams.

- We provide a proof of optimality for the projected block coordinate descent solutions in the analog beamforming design. Such proof allows us to establish important insights on the guaranteed convergence of the proposed algorithm, which is further supported by additional numerical simulation results.
- Finally, we provide extensive numerical simulation results to confirm the effectiveness of the proposed design. The experiments consider a wide range of operation scenarios for both Rayleigh and mmWave channel models, as well as practical constraints, such as quantized PS and channel estimation errors. The simulation results show that the proposed method outperforms other HBF designs in the literature.

C. ORGANIZATION AND NOTATIONS

This article is organized as follows. We introduce the multiuser massive MIMO system model, the channel models, and the problem formulation in Section II. In Section III, we present the proposed HBF design and address its computational complexity. Simulation results, convergence analysis and discussions are presented in Section IV; and finally, we draw our conclusions in Section V.

Throughout the paper, we adopt non-bold, boldfaced lower-case, and boldfaced upper-case letters, respectively, for scalars, vectors, and matrices. $\mathbb{E}[\,\cdot\,]$, $(\cdot)^{\mathrm{T}}$, and $(\cdot)^{\mathrm{H}}$ denote, respectively, the expectation, the transpose, and the conjugate transpose; $|\cdot|$, $\|\cdot\|$, and $\|\cdot\|_{\mathrm{F}}$ denote, respectively, the scalar modulus or matrix determinant, vector norm, and Frobenius norm; $\mathrm{tr}\{\cdot\}$ is the trace of a matrix and $\mathrm{blkdiag}\{\mathbf{A}_1, \ldots, \mathbf{A}_N\}$ represents a block diagonal matrix with diagonal block entries $\mathbf{A}_1, \ldots, \mathbf{A}_N$; $\mathbf{I}_M$ is an M-dimensional identity matrix, $[\mathbf{v}]_m$ represents the m-th element of vector $\mathbf{v}$, and $\mathbf{A}(m, n)$ is the entry in the m-th row and n-th column of $\mathbf{A}$.

II. SYSTEM MODEL AND PROBLEM FORMULATION

In this section, we present the multiuser system model, the channel model, and our problem formulation.

A. SYSTEM MODEL

We consider the downlink of a MU-MIMO narrowband massive MIMO system with HBF structure, as depicted in Fig. 1, in which a base-station (BS) having N_{t} antenna elements and $N_{\mathrm{t}}^{\mathrm{RF}}$ RF chains simultaneously communicates with K users. Each user is equipped with N_{r} antenna elements and $N_{\mathrm{r}}^{\mathrm{RF}}$ RF-chains and supports N_{s} data-streams. To ensure effective multi-stream communication, the system must satisfy $N_{\mathrm{s}} \leq N_{\mathrm{r}}^{\mathrm{RF}} \leq N_{\mathrm{r}}$ and $KN_{\mathrm{s}} \leq N_{\mathrm{t}}^{\mathrm{RF}} \leq N_{\mathrm{t}}$. At the BS, the hybrid precoder consists of a digital precoder matrix $\mathbf{F}_{\mathrm{BB}} \in \mathbb{C}^{N_{\mathrm{t}}^{\mathrm{RF}} \times KN_{\mathrm{s}}}$ and an analog precoder matrix $\mathbf{F}_{\mathrm{RF}} \in \mathbb{C}^{N_{\mathrm{t}} \times N_{\mathrm{t}}^{\mathrm{RF}}}$. The analog precoder is implemented using phase shifters, and thus imposes a constant modulus constraint (i.e., $|\mathbf{F}_{\mathrm{RF}}(m, n)| = 1/\sqrt{N_{\mathrm{t}}}\ \ \forall m, n$). We assume that the symbol vector $\mathbf{s} = [\mathbf{s}_1^{\mathrm{T}}, \mathbf{s}_2^{\mathrm{T}}, \ldots, \mathbf{s}_K^{\mathrm{T}}]^{\mathrm{T}} \in \mathbb{C}^{KN_{\mathrm{s}} \times 1}$, where $\mathbf{s}_k \in \mathbb{C}^{N_{\mathrm{s}} \times 1}$ refers to the symbols of the k-th user, has with unity variance and independent components, i.e., $\mathbb{E}[\mathbf{s}\mathbf{s}^{\mathrm{H}}] = \frac{1}{KN_{\mathrm{s}}}\mathbf{I}_{KN_{\mathrm{s}}}$. The symbol vector is precoded in the digital and analog domain before being transmitted, so that the transmitted signal is given by

$$\mathbf{x} = \mathbf{F}_{\mathrm{RF}}\mathbf{F}_{\mathrm{BB}}\mathbf{P}\mathbf{s} \tag{1}$$

where $\mathbf{x} \in \mathbb{C}^{N_{\mathrm{t}} \times 1}$, $\mathbf{P} \in \mathbb{D}^{KN_{\mathrm{s}} \times KN_{\mathrm{s}}}$ is the diagonal power allocation matrix, with total transmitted power $P_{\mathrm{t}} = \|\mathbf{P}\|_{\mathrm{F}}^2$, and $\|\mathbf{F}_{\mathrm{RF}}\mathbf{F}_{\mathrm{BB}}\|_{\mathrm{F}}^2 = KN_{\mathrm{s}}$.

We assume the signal is transmitted over a narrowband flat-fading channel $\mathbf{H}_k \in \mathbb{C}^{N_{\mathrm{r}} \times N_{\mathrm{t}}}$, where $\mathbf{H}_k$ represents the channel matrix of the k-th user. Thus, the signal received at the k-th user antennas, $\mathbf{y}_k \in \mathbb{C}^{N_{\mathrm{r}} \times 1}$, is

$$\mathbf{y}_k = \mathbf{H}_k\mathbf{F}_{\mathrm{RF}}\mathbf{F}_{\mathrm{BB}}\mathbf{P}\mathbf{s} + \mathbf{n}_k \tag{2}$$

where $\mathbf{n}_k \in \mathbb{C}^{N_{\mathrm{r}} \times 1}$ is the noise vector, such that $\mathbf{n}_k$ is i.i.d. $\mathcal{CN}(\mathbf{0}, \sigma_{\mathrm{n}}^2\mathbf{I}_{N_{\mathrm{r}}})$. At the k-th user, the received signal $\mathbf{y}_k$ is first processed by the analog combiner matrix $\mathbf{W}_{\mathrm{RF},k} \in \mathbb{C}^{N_{\mathrm{r}} \times N_{\mathrm{r}}^{\mathrm{RF}}}$, downconverted, and then processed by

the digital combiner matrix $\mathbf{W}_{\mathrm{BB},k} \in \mathbb{C}^{N_{\mathrm{r}}^{\mathrm{RF}} \times N_{\mathrm{s}}}$. The analog combiner is also implemented using phase shifters, and thus is constrained to have constant modulus, such that $|\mathbf{W}_{\mathrm{RF},k}(m,n)| = 1/\sqrt{N_{\mathrm{r}}}\ \forall m,n$. The received symbol is expressed by

$$\hat{\mathbf{s}}_k = \mathbf{W}_{\mathrm{BB},k}^{\mathrm{H}} \mathbf{W}_{\mathrm{RF},k}^{\mathrm{H}} \mathbf{H}_k \mathbf{F}_{\mathrm{RF}} \mathbf{F}_{\mathrm{BB}} \mathbf{s} + \mathbf{W}_{\mathrm{BB},k}^{\mathrm{H}} \mathbf{W}_{\mathrm{RF},k}^{\mathrm{H}} \mathbf{n}_k. \quad (3)$$

We define the aggregated multiuser channel as $\mathbf{H} = [\mathbf{H}_1^{\mathrm{T}}\ \mathbf{H}_2^{\mathrm{T}}\ \cdots\ \mathbf{H}_K^{\mathrm{T}}]^{\mathrm{T}}$, the aggregated analog combining matrix as $\mathbf{W}_{\mathrm{RF}} = \mathrm{blkdiag}\{\mathbf{W}_{\mathrm{RF},1}, \ldots, \mathbf{W}_{\mathrm{RF},K}\}$, and the baseband effective channel of the k-th user as $\bar{\mathbf{H}}_k = \mathbf{W}_{\mathrm{RF},k}^{\mathrm{H}} \mathbf{H}_k \mathbf{F}_{\mathrm{RF}} \in \mathbb{C}^{N_{\mathrm{r}}^{\mathrm{RF}} \times N_{\mathrm{t}}^{\mathrm{RF}}}$. Thus, we can represent the entire multiuser baseband effective channel $\mathbf{H}_{\mathrm{eff}} = [\bar{\mathbf{H}}_1^{\mathrm{T}}\ \bar{\mathbf{H}}_2^{\mathrm{T}}\ \cdots\ \bar{\mathbf{H}}_K^{\mathrm{T}}]^{\mathrm{T}}$ as

$$\begin{aligned}\mathbf{H}_{\mathrm{eff}} &= \mathbf{W}_{\mathrm{RF}}^{\mathrm{H}} \mathbf{H} \mathbf{F}_{\mathrm{RF}} \\ &= \begin{bmatrix} \mathbf{W}_{\mathrm{RF},1}^{\mathrm{H}} & \mathbf{0} & \cdots & \mathbf{0} \\ \mathbf{0} & \mathbf{W}_{\mathrm{RF},2}^{\mathrm{H}} & \cdots & \mathbf{0} \\ \vdots & \vdots & \ddots & \vdots \\ \mathbf{0} & \mathbf{0} & \cdots & \mathbf{W}_{\mathrm{RF},K}^{\mathrm{H}} \end{bmatrix} \begin{bmatrix} \mathbf{H}_1 \\ \mathbf{H}_2 \\ \vdots \\ \mathbf{H}_K \end{bmatrix} \mathbf{F}_{\mathrm{RF}}. \quad (4)\end{aligned}$$

The estimated symbol for the i-th data stream in the k-th user, $\hat{s}_{k_i}$, can be expressed as [30]

$$\begin{aligned}\hat{s}_{k_i} &= \sqrt{P_{k_i}} \mathbf{W}_{\mathrm{BB},k}^{\mathrm{H}}(i,:) \bar{\mathbf{H}}_k \mathbf{F}_{\mathrm{BB}}(:,k_i) s_{k_i} \\ &\quad + \sum_{j=1, j\neq i}^{N_s} \sqrt{P_{k_j}} \mathbf{W}_{\mathrm{BB},k}^{\mathrm{H}}(i,:) \bar{\mathbf{H}}_k \mathbf{F}_{\mathrm{BB}}(:,k_j) s_{k_j} \\ &\quad + \sum_{m=1, m\neq k}^{K} \sum_{l=1}^{N_s} \sqrt{P_{m_l}} \mathbf{W}_{\mathrm{BB},k}^{\mathrm{H}}(i,:) \bar{\mathbf{H}}_k \mathbf{F}_{\mathrm{BB}}(:,m_l) s_{m_l} \\ &\quad + \mathbf{W}_{\mathrm{BB},k}^{\mathrm{H}}(i,:) \mathbf{W}_{\mathrm{RF},k}^{\mathrm{H}} \mathbf{n}_k \quad (5)\end{aligned}$$

where $k_i = (k-1)N_s + i$, s_{k_i} is the i-th element of $\mathbf{s}_k$ and P_{k_i} is the power allocated to the i-th data stream of the k-th user.

Considering that Gaussian symbols are transmitted, the achievable sum-rate is

$$R_{\mathrm{sum}} = \sum_{k=1}^{K} \sum_{i=1}^{N_s} \log_2\left(1 + \mathrm{SINR}_{k_i}\right) \quad (6)$$

where SINR_{k_i} represents the signal-to-interference-plus-noise ratio of the i-th data stream of the k-th user, given by

$$\mathrm{SINR}_{k_i} = \frac{\mathrm{S}}{\mathrm{I} + \mathrm{N}} \quad (7)$$

with S, I, and N being, respectively, the signal, interference, and noise power, given by

$$\begin{aligned}\mathrm{S} &= \frac{P_{k_i}}{K N_{\mathrm{s}}} \left\| \mathbf{W}_{\mathrm{BB},k}^{\mathrm{H}}(i,:) \bar{\mathbf{H}}_k \mathbf{F}_{\mathrm{BB}}(:,k_i) \right\|^2 \\ \mathrm{I} &= \sum_{j=1, j\neq i}^{N_s} \frac{P_{k_j}}{K N_{\mathrm{s}}} \left\| \mathbf{W}_{\mathrm{BB},k}^{\mathrm{H}}(i,:) \bar{\mathbf{H}}_k \mathbf{F}_{\mathrm{BB}}(:,k_j) \right\|^2 \\ &\quad + \sum_{m=1, m\neq k}^{K} \sum_{l=1}^{N_s} \frac{P_{m_l}}{K N_{\mathrm{s}}} \left\| \mathbf{W}_{\mathrm{BB},k}^{\mathrm{H}}(i,:) \bar{\mathbf{H}}_k \mathbf{F}_{\mathrm{BB}}(:,m_l) \right\|^2 \\ \mathrm{N} &= \sigma_{\mathrm{n}}^2 \left\| \mathbf{W}_{\mathrm{RF},k} \mathbf{W}_{\mathrm{BB},k}(i,:) \right\|_{\mathrm{F}}^2.\end{aligned}$$

B. CHANNEL MODEL

We consider a generic channel model $\mathbf{H}_k = \sqrt{\rho_k} \dot{\mathbf{H}}_k$, where $\sqrt{\rho_k}$ and $\dot{\mathbf{H}}_k$ model, respectively, the large scale fading and the fast fading, satisfying $\mathbb{E}[\|\dot{\mathbf{H}}_k\|_{\mathrm{F}}^2] = N_{\mathrm{r}} N_{\mathrm{t}}$. Two distinct fast fading models are considered herein: the Rayleigh model, which represents a rich scattering environment, and the Saleh-Valenzuela model, which represents the sparse scattering environment of mmWave channels. In the Rayleigh model, each entry of the fast fading channel matrix $\dot{\mathbf{H}}_k$ follows an i.i.d. zero mean complex Gaussian distribution, i.e., $\dot{\mathbf{H}}_k(m,n) \sim \mathcal{CN}(0,1)$.

The Saleh-Valenzuela channel model, on the other hand, corresponds to the sum of the contributions of N_{cl} scattering clusters, each formed by N_{ray} propagation paths. The discrete-time narrowband flat-fading channel matrix of the k-th user is given by [17]

$$\mathbf{H}_k = \sqrt{\frac{N_{\mathrm{r}} N_{\mathrm{t}}}{N_{\mathrm{cl}} N_{\mathrm{ray}}}} \sum_{i=0}^{N_{\mathrm{cl}}-1} \sum_{l=0}^{N_{\mathrm{ray}}-1} \alpha_{il} \mathbf{a}_{\mathrm{r}}\left(\phi_{il}^{\mathrm{r}}, \theta_{il}^{\mathrm{r}}\right) \mathbf{a}_{\mathrm{t}}^{\mathrm{H}}\left(\phi_{il}^{\mathrm{t}}, \theta_{il}^{\mathrm{t}}\right), \quad (8)$$

where α_{il} corresponds to the complex gain of the l-th multipath ray in the i-th cluster, the vectors $\mathbf{a}_{\mathrm{r}}(\phi_{il}^{\mathrm{r}}, \theta_{il}^{\mathrm{r}})$ and $\mathbf{a}_{\mathrm{t}}(\phi_{il}^{\mathrm{t}}, \theta_{il}^{\mathrm{t}})$ are the array response vectors of the receiver and transmitter, respectively, whereas ϕ_{il}^{t} and θ_{il}^{t} are the azimuth and elevation angles of departure (AoD), and ϕ_{il}^{r} and θ_{il}^{r} are the azimuth and elevation angles of arrival (AoA). The complex gain α_{il} is assumed i.i.d. $\mathcal{CN}(0, \sigma_{\alpha,i}^2)$, where $\sigma_{\alpha,i}^2$ is the average power of the i-th cluster. The average cluster powers are such that $\sum_{i=1}^{N_{\mathrm{cl}}} \sigma_{\alpha,i}^2 = \sqrt{N_{\mathrm{r}} N_{\mathrm{t}} / N_{\mathrm{cl}} N_{\mathrm{ray}}}$. The azimuth and elevation angles of departure $\phi_{il}^{\mathrm{t}}, \theta_{il}^{\mathrm{t}}$ and arrival $\phi_{il}^{\mathrm{r}}, \theta_{il}^{\mathrm{r}}$ for the N_{ray} paths in the i-th cluster are modeled as Laplacian distributed random variable, with mean $\phi_i^{\mathrm{t}}, \theta_i^{\mathrm{t}}, \phi_i^{\mathrm{r}}, \theta_i^{\mathrm{r}}$ uniformly-distributed over $[-\pi, \pi)$, and angular spread of $\sigma_\phi^{\mathrm{t}}, \sigma_\theta^{\mathrm{t}}, \sigma_\phi^{\mathrm{r}}, \sigma_\theta^{\mathrm{r}}$, respectively. We consider a $\sqrt{N} \times \sqrt{N}$ uniform square planar array (USPA), with $N = N_{\mathrm{t}}$ or $N = N_{\mathrm{r}}$. The array response vector is defined as [18]

$$\begin{aligned}\mathbf{a}(\phi, \theta) = \frac{1}{\sqrt{N}} \Big[&1, \ldots, e^{j\frac{2\pi d}{\lambda}[h \sin(\phi)\sin(\theta) + v\cos(\theta)]}, \ldots, \\ &e^{j\frac{2\pi d}{\lambda}\left[(\sqrt{N}-1)\sin(\phi)\sin(\theta) + (\sqrt{N}-1)\cos(\theta)\right]} \Big]^{\mathrm{T}} \quad (9)\end{aligned}$$

where d and λ are the spacing between elements and the signal wavelength, respectively, and $0 \leq h < \sqrt{N} - 1$ and $0 \leq v < \sqrt{N} - 1$ are the indexes of the antenna element in the 2D plane.

C. PROBLEM FORMULATION

In this article, we aim to design hybrid precoders and combiners to maximize the achievable sum-rate of a MU-MIMO system. Such design problem is formulated as

$$\begin{aligned}\max_{\mathbf{F}_{\mathrm{RF}}, \mathbf{F}_{\mathrm{BB}}, \mathbf{W}_{\mathrm{RF},k}, \mathbf{W}_{\mathrm{BB},k}, \mathbf{P}} \quad & R_{\mathrm{sum}} \\ \text{s.t.} \quad & \mathbf{F}_{\mathrm{RF}} \in \mathcal{F}_{\mathrm{RF}} \\ & \mathbf{W}_{\mathrm{RF},k} \in \mathcal{W}_{\mathrm{RF}} \\ & \|\mathbf{F}_{\mathrm{RF}} \mathbf{F}_{\mathrm{BB}}\|_{\mathrm{F}}^2 = K N_{\mathrm{s}} \\ & \mathrm{tr}\{\mathbf{P}^{\mathrm{H}} \mathbf{P}\} = P_{\mathrm{t}} \quad (10)\end{aligned}$$

where $\mathcal{F}_{\mathrm{RF}}$ and $\mathcal{W}_{\mathrm{RF}}$ are, respectively, the set of all feasible analog precoder and combiner matrices (i.e., all $N_{\mathrm{t}} \times N_{\mathrm{t}}^{\mathrm{RF}}$ and $N_{\mathrm{r}} \times N_{\mathrm{r}}^{\mathrm{RF}}$ matrices with constant modulus entries), and $\|\mathbf{F}_{\mathrm{RF}}\mathbf{F}_{\mathrm{BB}}\|_{\mathrm{F}}^2 = KN_{\mathrm{s}}$, along with $\mathrm{tr}\{\mathbf{P}^{\mathrm{H}}\mathbf{P}\} = P_{\mathrm{t}}$, ensures the total transmitted power constraint. For simplicity, we assume $N_{\mathrm{t}}^{\mathrm{RF}} = KN_{\mathrm{r}}^{\mathrm{RF}} = KN_{\mathrm{s}}$. Nonetheless, we follow [17]–[32], by assuming that perfect channel state information (CSI) is available. Although perfect channel estimation with HBF architecture is very challenging, efficient methods have been presented in [34], [35], and references therein.

Note that solving problem (10) is very challenging as it requires a joint optimization over multiple variables subjected to the non-convex constant modulus constraint imposed by the phase-shifters network in the analog beamforming. In fact, the HBF design for attaining the global optimum sum-rate is found to be intractable even for the single-user system [17]. Practical solutions often consider sub-optimal solutions, such as the two-stage approaches in which the analog and digital beamforming are designed separately. Moreover, in most of these approaches, the analog beamforming is designed to enhance the effective baseband channel gain, regardless of the interference.

III. PROPOSED HYBRID BEAMFORMING DESIGN

The optimal solution to the sum-rate maximization problem for MU-MIMO system requires the effective channel to be diagonal or at least near-diagonal in order to ensure that the inter and intra-user interferences are suppressed [33]. In fully-digital MU-MIMO systems, the channel diagonalization is attained by designing the precoder and combiner with the BD scheme. For HBF systems, on the other hand, the channel diagonalization can be achieved by designing BD digital precoder and combiner, while the analog precoder and combiner provide an extra degree-of-freedom – often used for harvesting array gain.

Here, we propose a novel hybrid precoder and combiner design for multiuser mmWave massive MIMO. The proposed design consists of two stages, where we jointly design the analog precoder and combiner for all users in the first stage, and then use the effective baseband channel to design the digital beamforming in the second stage. Differently from previous designs, we explore the extra degree-of-freedom provided by the analog beamforming not only to harvest the array gain, but also to provide intra- and inter-user interference suppression. The digital beamforming is designed using the regularized channel diagonalization approach (RCD) [32]. In the following subsections, we describe the proposed analog beamforming design, the digital RCD approach, and the computational complexity of the proposed method.

A. ANALOG PRECODER AND COMBINER DESIGN

To design the analog precoder and combiner, we aim to diagonalize the effective baseband channel $\mathbf{H}_{\mathrm{eff}}$, such that the effective gain of each data stream is maximized while the interference among different data streams is suppressed. This problem is equivalent to finding the best rank-KN_{s} channel approximation $\mathbf{H} \approx \mathbf{W}_{\mathrm{RF}}\mathbf{\Sigma}\mathbf{F}_{\mathrm{RF}}^{\mathrm{H}}$, so that $\mathbf{H}_{\mathrm{eff}} = \mathbf{W}_{\mathrm{RF}}^{\mathrm{H}}\mathbf{H}\mathbf{F}_{\mathrm{RF}} \approx \mathbf{\Sigma}$, where $\mathbf{\Sigma}$ is a $KN_{\mathrm{s}} \times KN_{\mathrm{s}}$ diagonal matrix while both $\mathbf{W}_{\mathrm{RF}}$ and $\mathbf{F}_{\mathrm{RF}}^{\mathrm{H}}$ are orthonormal. After taking the hardware constraints associated with the analog precoder and combiner into account, the design problem is formulated as

$$\begin{aligned} \min_{\mathbf{F}_{\mathrm{RF}},\, \mathbf{W}_{\mathrm{RF}},\, \mathbf{\Sigma}} \quad & \left\|\mathbf{H} - \mathbf{W}_{\mathrm{RF}}\mathbf{\Sigma}\mathbf{F}_{\mathrm{RF}}^{\mathrm{H}}\right\|_{\mathrm{F}}^2 \\ \text{s.t.} \quad & \mathbf{W}_{\mathrm{RF}}^{\mathrm{H}}\mathbf{W}_{\mathrm{RF}} = \mathbf{I}_{KN_{\mathrm{s}}} \\ & \mathbf{F}_{\mathrm{RF}}^{\mathrm{H}}\mathbf{F}_{\mathrm{RF}} = \mathbf{I}_{KN_{\mathrm{s}}} \\ & \mathbf{W}_{\mathrm{RF}} = \mathrm{blkdiag}\left\{\mathbf{W}_{\mathrm{RF},1}, \ldots, \mathbf{W}_{\mathrm{RF},K}\right\} \\ & \mathbf{W}_{\mathrm{RF},k} \in \mathcal{W}_{\mathrm{RF}} \\ & \mathbf{F}_{\mathrm{RF}} \in \mathcal{F}_{\mathrm{RF}}. \end{aligned} \tag{11}$$

Note that the third constraint is imposed by the system model while the two last constraints correspond to the constant-modulus constraint imposed by the phase-shifters. Without these three constraints, the problem corresponds to the classical low-rank matrix approximation problem. With proper algebraic manipulation, the problem in (11) can be equivalently cast as [36], [37]

$$\begin{aligned} \max_{\mathbf{F}_{\mathrm{RF}},\, \mathbf{W}_{\mathrm{RF}}} \quad & \left\|\mathbf{W}_{\mathrm{RF}}^{\mathrm{H}}\mathbf{H}\mathbf{F}_{\mathrm{RF}}\right\|_{\mathrm{F}}^2 \\ \text{s.t.} \quad & \mathbf{W}_{\mathrm{RF}}^{\mathrm{H}}\mathbf{W}_{\mathrm{RF}} = \mathbf{I}_{KN_{\mathrm{s}}} \\ & \mathbf{F}_{\mathrm{RF}}^{\mathrm{H}}\mathbf{F}_{\mathrm{RF}} = \mathbf{I}_{KN_{\mathrm{s}}} \\ & \mathbf{W}_{\mathrm{RF}} = \mathrm{blkdiag}\{\mathbf{W}_{\mathrm{RF},1}, \ldots, \mathbf{W}_{\mathrm{RF},K}\} \\ & \mathbf{W}_{\mathrm{RF},k} \in \mathcal{W}_{\mathrm{RF}} \\ & \mathbf{F}_{\mathrm{RF}} \in \mathcal{F}_{\mathrm{RF}}. \end{aligned} \tag{12}$$

Owing to the non-convex constraints, the problem in (12) is found to be intractable. In order to overcome such a hurdle, we propose an heuristic algorithm for solving (12) through a series of KN_{s} successive rank-1 approximations, each corresponding to the design of one analog precoder and combiner vector pair. The rank-1 approximation problem is formulated as

$$\begin{aligned} \max_{\mathbf{f}_j, \mathbf{w}_j} \quad & \left|\mathbf{w}_j^{\mathrm{H}}\mathbf{H}\mathbf{f}_j\right| \\ \text{s.t.} \quad & \mathbf{f}_j^{\mathrm{H}}\mathbf{f}_j = 1 \\ & \mathbf{f}_j^{\mathrm{H}}\mathbf{f}_l = 0 \quad \forall j \neq l \\ & \mathbf{w}_j^{\mathrm{H}}\mathbf{w}_j = 1 \\ & \mathbf{w}_l^{\mathrm{H}}\mathbf{w}_l = 0 \quad \forall j \neq l \\ & \mathbf{W}_{\mathrm{RF}} = \mathrm{blkdiag}\left\{\mathbf{W}_{\mathrm{RF},1}, \ldots, \mathbf{W}_{\mathrm{RF},K}\right\} \\ & \left|[\mathbf{f}_j]_m\right| = 1/\sqrt{N_{\mathrm{t}}}, \ \forall m \in \{1, \ldots, N_{\mathrm{t}}\} \\ & \left|\left[\mathbf{w}_j\right]_n\right| = 1/\sqrt{N_{\mathrm{r}}}, \ \forall n \in \{1, \ldots, N_{\mathrm{r}}\} \end{aligned} \tag{13}$$

where $\mathbf{F}_{\mathrm{RF}} = [\mathbf{f}_1 \cdots \mathbf{f}_{KN_{\mathrm{s}}}]$, $\mathbf{W}_{\mathrm{RF}} = [\mathbf{w}_1 \cdots \mathbf{w}_{KN_{\mathrm{s}}}]$, and $\{j, l\} \in \{1, 2, \ldots, KN_{\mathrm{s}}\}$. The problem in (13) is still non-convex and difficult to solve.

Therefore, we further simplify (13) according to the following observations: i) the cost function and constraints

in (13) are invariant to rotations in $\mathbf{w}_i$ and $\mathbf{f}_i$, thereby replacing the cost function with $\mathrm{Re}(\mathbf{w}_i^{\mathrm{H}}\mathbf{H}_{\mathrm{res}}^{(i)}\mathbf{f}_i)$ will also lead to an optimal solution of (13); ii) given the block-diagonal structure of the aggregated analog combiner matrix, we only need to ensure orthogonality among analog combiner vectors within the same user and, in addition, each analog combiner vector only interacts with the channel matrix of the same user; lastly, iii) the orthogonality constraint, which guarantees the interference suppression, can be slightly relaxed since it can be further ensured by the digital precoder and combiner. Bearing these observations in mind, we relax problem (13) as

$$\begin{aligned}\max_{\mathbf{w}_{k,i},\mathbf{f}_{k,i}} \quad & \mathrm{Re}\Big(\mathbf{w}_{k,i}^{\mathrm{H}}\mathbf{H}_{\mathrm{res},k}^{(i)}\mathbf{f}_{k,i}\Big) \\ \text{s.t.} \quad & \big\|\mathbf{f}_{k,i}\big\| = 1 \\ & \big\|\mathbf{w}_{k,i}\big\| = 1 \\ & \big|\big[\mathbf{f}_{k,i}\big]_m\big| = 1/\sqrt{N_{\mathrm{t}}},\ \forall m \in \{1,\ldots,N_{\mathrm{t}}\} \\ & \big|\big[\mathbf{w}_{k,i}\big]_n\big| = 1/\sqrt{N_{\mathrm{r}}},\ \forall n \in \{1,\ldots,N_{\mathrm{r}}\}. \end{aligned} \tag{14}$$

where $\mathbf{f}_{k,i}$ is the $[(k-1)N_{\mathrm{s}}+i]$-th column of $\mathbf{F}_{\mathrm{RF}}$, $\mathbf{w}_{k,i}$ is the i-th column of $\mathbf{W}_{\mathrm{RF},k}$, with $i \in \{1,\ldots,N_{\mathrm{s}}\}$ and $k \in \{1,\ldots,K\}$, such that $\mathbf{f}_{k,i}$ and $\mathbf{w}_{k,i}$ are, respectively, the analog precoder and analog combiner corresponding to the i-th data stream in the k-th user. Note that, in order to preserve some level of orthogonality, the channel matrix in (13) has been replaced with the residual channel matrix $\mathbf{H}_{\mathrm{res}}^{(i)}$, i.e., the channel matrix subtracted the contributions of the previously computed analog precoder and combiner vectors. In particular, $\mathbf{H}_{\mathrm{res},k}^{(i)}$ represents the residual channel matrix from the k-th user.

The solution to problem (14) is obtained with the projected block coordinate descent method [38], [39], by cyclically seeking the block coordinate descent solution with respect to each block variable (e.g., $\mathbf{w}_{k,i}$ or $\mathbf{f}_{k,i}$), while keeping the other block variable fixed. Thereby, we solve each block coordinate problem by relaxing the non-convex constant modulus constraint, and then, projecting the relaxed solution onto the non-convex set of constant modulus vectors. The solutions to the relaxed block coordinate descent problems are, respectively, given as

$$\hat{\mathbf{w}}_{k,i} = \frac{\mathbf{H}_{\mathrm{res},k}^{(i)}\mathbf{f}_{k,i}}{\Big\|\mathbf{H}_{\mathrm{res},k}^{(i)}\mathbf{f}_{k,i}\Big\|} \quad \text{and} \quad \hat{\mathbf{f}}_{k,i} = \frac{\mathbf{H}_{\mathrm{res},k}^{(i)^{\mathrm{H}}}\mathbf{w}_{k,i}}{\Big\|\mathbf{H}_{\mathrm{res},k}^{(i)^{\mathrm{H}}}\mathbf{w}_{k,i}\Big\|} \tag{15}$$

and the projection of the relaxed solutions onto the constant modulus vector space are obtained by extracting the phases of the relaxed solutions, i.e., by making

$$\mathbf{w}_{k,i} = \frac{1}{\sqrt{N_{\mathrm{r}}}}e^{j\angle\mathbf{H}_{\mathrm{res},k}^{(i)}\mathbf{f}_{k,i}} \quad \text{and} \quad \mathbf{f}_{k,i} = \frac{1}{\sqrt{N_{\mathrm{t}}}}e^{j\angle\mathbf{H}_{\mathrm{res},k}^{(i)^{\mathrm{H}}}\mathbf{w}_{k,i}}. \tag{16}$$

Note that, despite the non-convexity of the block coordinate problems, in the Appendix, we prove that the solutions in (16) are, in fact, optimal. Finally, the solution to (14) is obtained by iterating the equations in (16) until convergence.

After obtaining the pair of analog precoder and combiner vectors, the residual channel matrix for the k-th user is updated by simultaneously projecting the columns of $\mathbf{H}_{\mathrm{res},k}^{(i)}$ onto the subspace orthogonal to the analog combiner $\mathbf{w}_{k,i}$ and their rows onto the subspace orthogonal to the analog precoder $\mathbf{f}_{k,i}$ by making

$$\mathbf{H}_{\mathrm{res},k}^{(\gamma+1)} = \big(\mathbf{I}_{N_{\mathrm{r}}} - \mathbf{w}_{k,i}\mathbf{w}_{k,i}^{\mathrm{H}}\big)\mathbf{H}_{\mathrm{res},k}^{(\gamma)}\big(\mathbf{I}_{N_{\mathrm{t}}} - \mathbf{f}_{k,i}\mathbf{f}_{k,i}^{\mathrm{H}}\big) \tag{17}$$

while the residual channel matrix for the remaining users are updated by projecting their rows onto the subspace orthogonal to the analog precoder $\mathbf{f}_{k,i}$ by

$$\mathbf{H}_{\mathrm{res},j}^{(\gamma+1)} = \mathbf{H}_{\mathrm{res},j}^{(\gamma)}\big(\mathbf{I}_{N_{\mathrm{t}}} - \mathbf{f}_{k,i}\mathbf{f}_{k,i}^{\mathrm{H}}\big),\ \forall j \in \{1,\ldots,K | j \neq k\}. \tag{18}$$

The update in (17) allows us to find the analog precoder and combiner vectors for the $(i+1)$-th data stream in the k-th user that are, respectively, nearly-orthogonal to the analog precoder and combiner vectors for the i-th data stream of the same user. The update in (18), on the other hand, allows us to seek analog precoders for the remaining users that are nearly-orthogonal to the analog precoder computed for the i-th data stream in the k-th user. Note that finding orthogonal analog precoders and combiners is very difficult when we take into account the constant modulus constraints. Nonetheless, while the updates in (17) and (18) cannot assure orthogonality among the analog beamforming vectors, the near-orthogonality is good enough to provide intra- and inter-user interference reduction. The procedure for solving (14) described herein is repeated until the analog beamforming for all users and data streams are designed. The proposed algorithm is summarized in Algorithm 1.

Note that different user scheduling schemes can be adopted when solving the successive rank-one approximation problem in (14). In Algorithm 1, we seek fairness among the users and, therefore, we design the analog precoder and combiner vector pairs for one data stream in every user at a time. An additional possibility is to follow certain user priority scheme, thereby designing all the analog precoder and combiner vector pairs for the highest priority users to the lowest ones.

B. DIGITAL PRECODER AND COMBINER DESIGN

Having computed the analog precoder and combiner using Algorithm 1, the digital precoder and combiner are obtained by the regularized channel diagonalization (RCD) [32] of the baseband effective channel, defined in (4). Our goal is to reduce the MUI plus noise and to optimize the system performance. Therefore, in order to simplify the design, we adopt a two-step approach: first we address the MUI plus noise reduction, and then, the intra-user interference suppression and performance optimization. The later also allows us to obtain the digital combiner for every user. The digital precoder is written as

$$\mathbf{F}_{\mathrm{BB}} = \beta\mathbf{F}_{\mathrm{m}}\mathbf{F}_{\mathrm{p}} \tag{19}$$

with $\mathbf{F}_{\mathrm{m}} = [\mathbf{F}_{\mathrm{m}_1}\ \mathbf{F}_{\mathrm{m}_2}\ \cdots\ \mathbf{F}_{\mathrm{m}_K}] \in \mathbb{C}^{KN_{\mathrm{s}}\times KN_{\mathrm{s}}}$ and

Algorithm 1: Multiuser Joint Analog Precoder & Combiner Design

Initialize $\gamma = 0$ and $\mathbf{F}_{\mathrm{RF}} = [\ ]$
Initialize $\mathbf{W}_{\mathrm{RF},k} = [\ ]$ and $\mathbf{H}_{\mathrm{res},k}^{(0)} = \mathbf{H}_k, \forall k = 1, \cdots, K$
for $i = 1{:}N_{\mathrm{s}}$ **do**
  for $k = 1{:}K$ **do**
    Initialize $\mathbf{w}_{k,i}$ and $\mathbf{f}_{k,i}$ randomly
    Initialize $\eta = 0$; $\delta^{(0)} = 1$; $\delta^{(1)} = 0$
    while $|\delta^{(\eta+1)} - \delta^{(\eta)}| \geq \varepsilon$ **do**
      $\eta = \eta + 1$
      $\hat{\mathbf{w}}_{k,i} = \mathbf{H}_{\mathrm{res},k}^{(\gamma)} \mathbf{f}_{k,i}$
      $\mathbf{w}_{k,i} = (1/\sqrt{N_{\mathrm{r}}}) e^{j\angle \hat{\mathbf{w}}_{k,i}}$
      $\hat{\mathbf{f}}_{k,i} = \mathbf{H}_{\mathrm{res},k}^{(\gamma)\mathrm{H}} \mathbf{w}_{k,i}$
      $\mathbf{f}_{k,i} = (1/\sqrt{N_{\mathrm{t}}}) e^{j\angle \hat{\mathbf{f}}_{k,i}}$
      $\delta^{(\eta+1)} = \mathbf{w}_{k,i}^{\mathrm{H}} \mathbf{H}_{\mathrm{res},k}^{(\gamma)} \mathbf{f}_{k,i}$
    end
    $\mathbf{H}_{\mathrm{res},k}^{(\gamma+1)} = (\mathbf{I}_{N_{\mathrm{r}}} - \mathbf{w}_{k,i}\mathbf{w}_{k,i}^{\mathrm{H}}) \mathbf{H}_{\mathrm{res},k}^{(\gamma)} (\mathbf{I}_{N_{\mathrm{t}}} - \mathbf{f}_{k,i}\mathbf{f}_{k,i}^{\mathrm{H}})$
    for $j = 1 : K,\ j \neq k$ **do**
      $\mathbf{H}_{\mathrm{res},j}^{(\gamma+1)} = \mathbf{H}_{\mathrm{res},j}^{(\gamma)} (\mathbf{I}_{N_{\mathrm{t}}} - \mathbf{f}_{k,i}\mathbf{f}_{k,i}^{\mathrm{H}})$
    end
    $\mathbf{W}_{\mathrm{RF},k}(:, i) = \mathbf{w}_{k,i}$
    $\mathbf{F}_{\mathrm{RF}}(:, (k-1)N_{\mathrm{s}} + i) = \mathbf{f}_{k,i}$
    $\gamma = \gamma + 1$
  end
end
return $\mathbf{F}_{\mathrm{RF}}, \mathbf{W}_{\mathrm{RF}}$

$$\mathbf{F}_{\mathrm{p}} = \begin{bmatrix} \mathbf{F}_{\mathrm{p}_1} & \cdots & \mathbf{0} \\ \vdots & \ddots & \vdots \\ \mathbf{0} & \cdots & \mathbf{F}_{\mathrm{p}_K} \end{bmatrix} \in \mathbb{C}^{KN_{\mathrm{s}} \times KN_{\mathrm{s}}}$$

where $\mathbf{F}_{\mathrm{m}_k} \in \mathbb{C}^{KN_{\mathrm{s}} \times N_{\mathrm{s}}}$ is the primary digital precoder for MUI plus noise suppression, $\mathbf{F}_{\mathrm{p}_k} \in \mathbb{C}^{N_{\mathrm{s}} \times N_{\mathrm{s}}}$ is secondary digital precoder, used for performance optimization, and β is chosen to fulfill the total transmit power constraint in (10).

Therefore, we start by designing $\mathbf{F}_{\mathrm{m}}$ to minimize the MUI plus noise. First, we define $\tilde{\mathbf{H}}_k = [\bar{\mathbf{H}}_1^{\mathrm{T}} \cdots \bar{\mathbf{H}}_{k-1}^{\mathrm{T}} \bar{\mathbf{H}}_{k+1}^{\mathrm{T}} \cdots \bar{\mathbf{H}}_K^{\mathrm{T}}]^{\mathrm{T}} \in \mathbb{C}^{(K-1)N_{\mathrm{s}} \times KN_{\mathrm{s}}}$, such that $\|\tilde{\mathbf{H}}_k \mathbf{F}_{\mathrm{m}_k}\|_{\mathrm{F}}$ relates to the level of interference imposed by the k-th user to the remaining users. The design of $\mathbf{F}_{\mathrm{m}}$ is formulated as

$$\min_{\mathbf{F}_{\mathrm{m}}} \ \mathrm{E}\left\{ \sum_{k=1}^{K} \left\| \tilde{\mathbf{H}}_k \mathbf{F}_{\mathrm{m}_k} \right\|_{\mathrm{F}}^2 + \frac{\|\mathbf{n}\|^2}{\beta^2} \right\} \tag{20}$$

where $\mathbf{n} = [\mathbf{n}_1^{\mathrm{T}} \cdots \mathbf{n}_K^{\mathrm{T}}]^{\mathrm{T}}$. We further assume that all additive white Gaussian noise vector $\mathbf{n}_k$, for $k \in \{1, \ldots, K\}$ have the same variance σ_{n}^2. Thus, the problem in (20) can be written as [40, Appendix]

$$\min_{\mathbf{F}_{\mathrm{m}}} \ \sum_{k=1}^{K} \mathrm{tr}\left[\mathbf{F}_{\mathrm{m}_k}^{\mathrm{H}} \left(\tilde{\mathbf{H}}_k^{\mathrm{H}} \tilde{\mathbf{H}}_k + \frac{KN_{\mathrm{s}}\sigma_{\mathrm{n}}^2}{P_{\mathrm{t}}} \mathbf{I}_{KN_{\mathrm{s}}} \right) \mathbf{F}_{\mathrm{m}_k} \right]. \tag{21}$$

The solution to problem (21) is given by [41]

$$\mathbf{F}_{\mathrm{m}_k} = \left(\tilde{\mathbf{H}}_k^{\mathrm{H}} \tilde{\mathbf{H}}_k + \frac{KN_{\mathrm{s}}\sigma_{\mathrm{n}}^2}{P_{\mathrm{t}}} \mathbf{I}_{KN_{\mathrm{s}}} \right)^{-1}. \tag{22}$$

Next, by assuming that the primary digital precoder is able to minimize all MUI (i.e., $\mathbf{H}\mathbf{F}_{\mathrm{m}}$ is block diagonal), the secondary digital precoder and the digital combiner are designed by optimizing K parallel SU-MIMO separately. Let the effective SU-MIMO channel for the k-th user $\bar{\mathbf{H}}_k \mathbf{F}_{\mathrm{m}_k}$ and its SVD $\bar{\mathbf{H}}_k \mathbf{F}_{\mathrm{m}_k} = \mathbf{U}_{\mathrm{s}} \Sigma_{\mathrm{s}} \mathbf{V}_{\mathrm{s}}^{\mathrm{H}}$, the optimal secondary digital precoder and digital combiner for the sum-rate maximization under total transmitted power constraint are given, respectively, by the N_{s} column vectors of $\mathbf{V}_{\mathrm{s}}$ and $\mathbf{U}_{\mathrm{s}}$ associated with the N_{s} largest singular values of $\bar{\mathbf{H}}_k \mathbf{F}_{\mathrm{m}_k}$, i.e.,

$$\mathbf{F}_{\mathrm{p}_k} = \mathbf{V}_{\mathrm{s}}[\ :\ , 1 : N_{\mathrm{s}}] \tag{23}$$

and

$$\mathbf{W}_{\mathrm{BB},k} = \mathbf{U}_{\mathrm{e}}[\ :\ , 1 : N_{\mathrm{s}}]. \tag{24}$$

In order to the digital precoder to satisfy $\|\mathbf{F}_{\mathrm{RF}}\mathbf{F}_{\mathrm{BB}}\|_{\mathrm{F}}^2 = KN_{\mathrm{s}}$, we scale the digital precoder by making

$$\mathbf{F}_{\mathrm{BB}} = \sqrt{\frac{KN_{\mathrm{s}}}{\left\| \mathbf{F}_{\mathrm{RF}}\mathbf{F}_{\mathrm{m}}\mathbf{F}_{\mathrm{p}} \right\|_{\mathrm{F}}^2}} \mathbf{F}_{\mathrm{m}}\mathbf{F}_{\mathrm{p}}. \tag{25}$$

Lastly, the optimal power allocation matrix $\mathbf{P}$ is designed by the water-filling power allocation with total transmit power P_{t}.

Note that the primary digital precoder for the k-th user in (22) transmits in the subspace spanned by all other users with power inversely proportional to $\tilde{\mathbf{H}}_k$'s singular values [40]. Therefore, the RCD design trades-off some of its MUI suppression capabilities for a better performance in low-SNR scenarios. For high SNR, the transmission tends to concentrate in the null-space of $\tilde{\mathbf{H}}_k$, and thus, the RCD precoder approaches the BD design.

C. COMPUTATIONAL COMPLEXITY

The iterative process used to design the analog precoder and combiner matrices has computational complexity order of $O\{KN_{\mathrm{s}}N_{\mathrm{t}}N_{\mathrm{r}}(N_{\mathrm{ite}}+K)\}$, where N_{ite} is the number of iterations required to compute an analog precoder and combiner vector pair. The design of the digital precoder and combiner requires the computation of the effective channel, with complexity $O\{KN_{\mathrm{s}}(N_{\mathrm{t}}N_{\mathrm{r}}+KN_{\mathrm{t}}N_{\mathrm{s}})\}$, the baseband RCD design with complexity $O\{K^4N_{\mathrm{s}}^3\}$, followed by the digital precoder normalization with complexity $O\{K^2N_{\mathrm{s}}^2N_{\mathrm{t}}\}$. Under the assumption that $N_{\mathrm{s}} \leq N_{\mathrm{r}}$ (which always hold for the proposed system), the overall complexity order of the proposed design is approximately $O\{KN_{\mathrm{s}}[K^3N_{\mathrm{s}}^2+N_{\mathrm{t}}N_{\mathrm{r}}(K+N_{\mathrm{ite}})]\}$. For comparison, the complexity order of the algorithms in [28]–[32] are presented in Table 1. Note that the proposed design has complexity comparable to the Hy-BD, EBC-HBF, and Hy-SBD, and much lower than the SP-BD-HBF and the HRCD designs.

TABLE 1. Computational complexity of MU-MIMO HBF design methods.

Method	Computational complexity
Prop. Method	$O\left\{KN_{\mathrm{s}}[K^3N_{\mathrm{s}}^2 + N_{\mathrm{t}}N_{\mathrm{r}}(K + N_{\mathrm{ite}})]\right\}$
Hy-BD [28]	$O\left\{K[K^3N_{\mathrm{s}}^3 + KN_{\mathrm{s}}^2N_{\mathrm{t}} + N_{\mathrm{t}}N_{\mathrm{r}}^2]\right\}$
SP-BD-HBF [29]	$O\left\{K[(KN_{\mathrm{cl}}N_{\mathrm{ray}})^3 + (KN_{\mathrm{cl}}N_{\mathrm{ray}})^2N_{\mathrm{t}} + (KN_{\mathrm{cl}}N_{\mathrm{ray}})N_{\mathrm{t}}^2 + N_{\mathrm{t}}^3 + (KN_{\mathrm{s}})^2N_{\mathrm{t}}]\right\}$
EBC-HBF [31]	$O\left\{KN_{\mathrm{s}}^2[K^3N_{\mathrm{s}} + KN_{\mathrm{s}}^2N_{\mathrm{t}} + N_{\mathrm{ite}}(N_{\mathrm{t}}^2 + N_{\mathrm{r}}^2)]\right\}$
Hy-SBD [30]	$O\left\{K[K^3N_{\mathrm{s}}^3 + KN_{\mathrm{s}}^2N_{\mathrm{t}} + N_{\mathrm{t}}N_{\mathrm{r}}^2]\right\}$
HRCD [32]	$O\left\{K[K^3N_{\mathrm{s}}^3 + KN_{\mathrm{s}}^2N_{\mathrm{t}} + N_{\mathrm{t}}N_{\mathrm{r}}^2 + N_{\mathrm{s}}N_{\mathrm{cl}}N_{\mathrm{ray}}]\right\}$

IV. SIMULATION RESULTS

In this section, we present simulation results to evaluate the performance of the proposed approach and compare with other methods in the literature. The results are obtained by averaging the achievable sum-rate over 1000 channel realizations, considering both the Rayleigh and the Saleh-Valenzuela (mmWave) channel models. The proposed approach is compared to the hybrid BD (Hy-BD) [28], subspace-projection-aided BD (Hy-SBD) [30], equivalent baseband channel HBF (EBF-HBF) [31], and hybrid regularized channel diagonalization (HRCD) [32]. The SVD-based fully-digital (FD-SVD) design in [30] is used as benchmark, as it provides a much better performance than the traditional fully digital BD. Note, however, that the FD-SVD is not capacity-achieving, and it is possible that HBF designs outperform the fully-digital design in some situations. The HRCD design requires the knowledge of the array response vectors for all propagation paths and thus, can only be deployed for the mmWave channel model. We adopt $\varepsilon = 0.001$ to control the convergence of Algorithm 1; and assume $\rho_k = 1 \forall k$ and the transmit SNR $= P_{\mathrm{t}}/\sigma_{\mathrm{n}}^2$.

A. RAYLEIGH CHANNEL

We start by considering the Rayleigh channel model. In the first experiment, we assume a MU-MIMO system with $N_{\mathrm{t}} = 144$ transmit antennas communicating to $K = 8$ users through $N_{\mathrm{s}} = 4$ data streams, with each user having $N_{\mathrm{r}} = 16$ receive antennas. We evaluate the achievable sum-rate over different SNR values in the range $[-20, 10]$ dB. The results, depicted in Fig. 2, show that the proposed method has outperformed all the other HBF designs, providing up to 3 bits/s/Hz improvement over the Hy-SBD.

In the second experiment, we evaluate the achievable sum-rate for different number of transmit antennas N_{t}. We assume a systems with $K = 4$ users, each having $N_{\mathrm{r}} = 16$ receive antennas and communicating through $N_{\mathrm{s}} = 4$ data streams, at SNR = -5 dB. The results in Fig. 3 show that the proposed design outperform the other HBF designs and can even outperform the fully-digital solution for a small number of transmit antennas. Next, we evaluate the achievable sum-rate for different number of data streams N_{s} for a 144×16 MU-MIMO system with $K = 4$ users at SNR = 5 dB. The proposed algorithm outperforms all other HBF designs, and

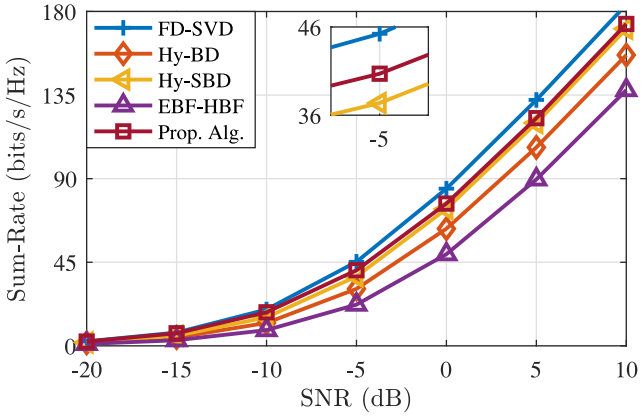

FIGURE 2. Sum-rate vs. SNR for $N_{\mathrm{t}} = 144$, $N_{\mathrm{r}} = 16$, $K = 8$, and $N_{\mathrm{S}} = 4$.

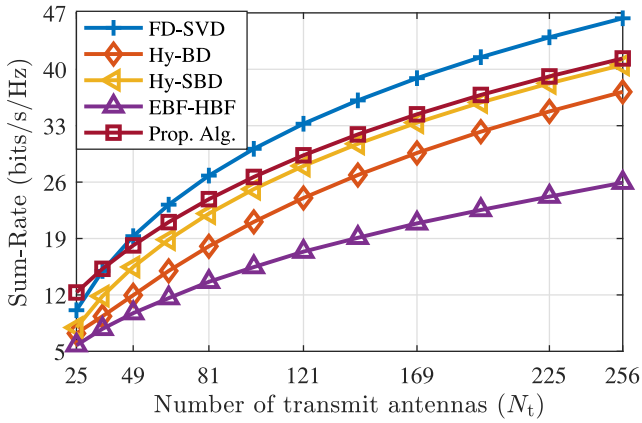

FIGURE 3. Sum-rate vs. number of transmit antennas N_{t} for $N_{\mathrm{r}} = 16$, $K = 4$, and $N_{\mathrm{S}} = 4$ at SNR = -5 dB.

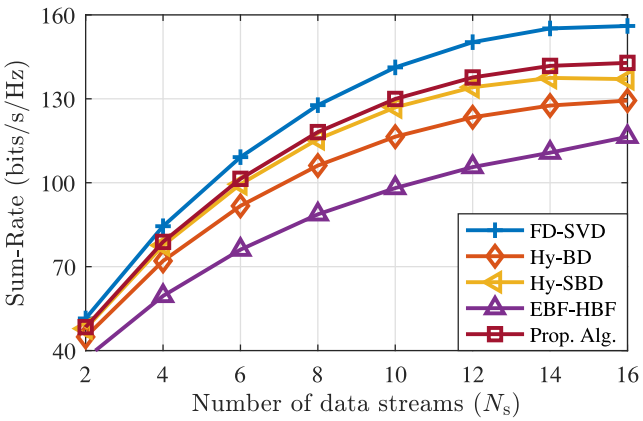

FIGURE 4. Sum-rate vs. number of data stream N_{S} for $N_{\mathrm{t}} = 144$, $N_{\mathrm{r}} = 16$, and $K = 4$ at SNR = 5 dB.

in the most critical scenario (i.e., $N_{\mathrm{s}} = 16$), it provides nearly 5.8 bits/s/Hz improvement over the Hy-SBD. The results are shown in Fig. 4.

In Fig. 5, we show the achievable sum-rate versus the number of users K. Here, we consider a 144×16 MU-MIMO system transmitting $N_{\mathrm{s}} = 4$ data streams at SNR $= -5$ dB. Once again, the proposed algorithm performs better than

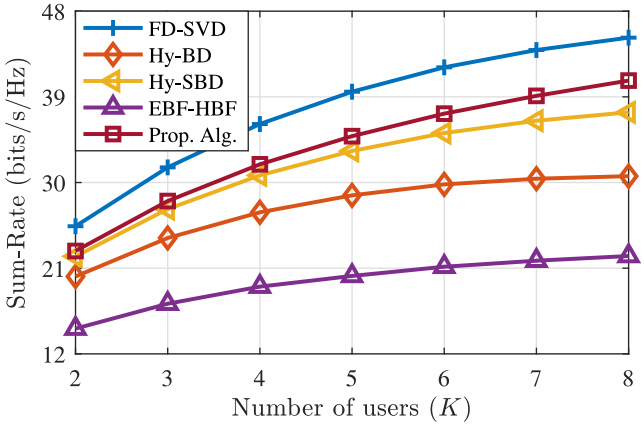

FIGURE 5. Sum-rate vs. number of users K for $N_t = 144$, $N_r = 16$, and $N_S = 4$ at SNR $= -5$ dB.

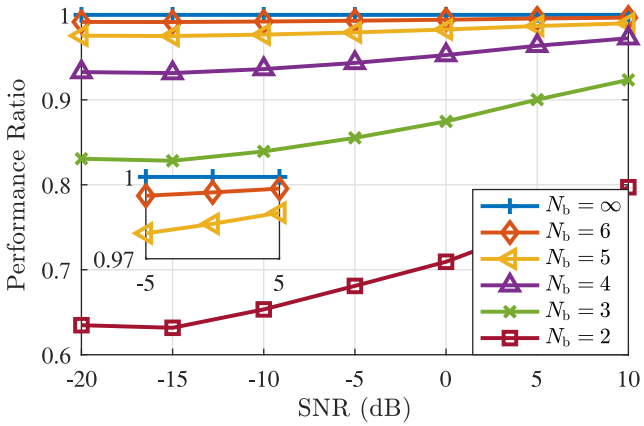

FIGURE 6. Ratio between sum-rate performance for quantized PS and non-quantized PS vs. SNR for different number of quantization bits N_b.

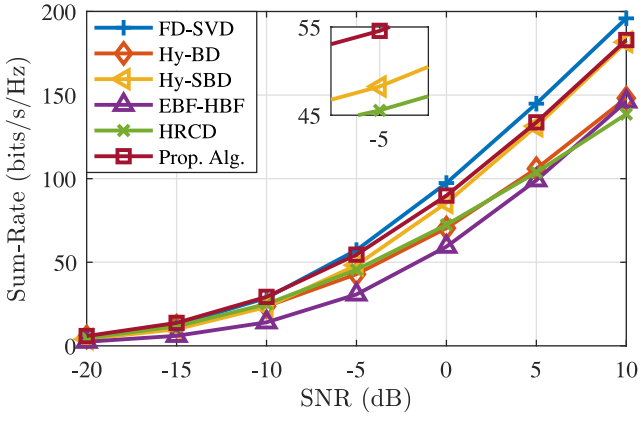

FIGURE 7. Sum-rate vs. SNR for $N_t = 144$, $N_r = 16$, $K = 8$, and $N_S = 4$.

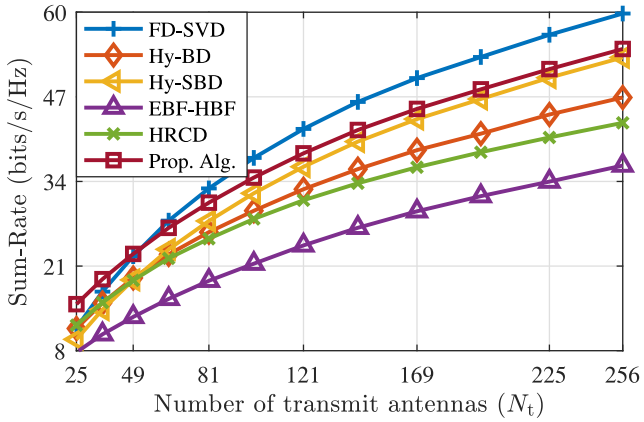

FIGURE 8. Sum-rate vs. number of transmit antennas N_t for $N_r = 16$, $K = 4$, and $N_S = 4$ at SNR $= -5$ dB.

the other designs. In the most critical case, i.e., $K = 8$, the improvement over the Hy-SBD reaches more than 3 bits/s/Hz.

Finally, we investigate the effects of the PS quantization. In the previous simulations, we have considered only non-quantized (i.e., infinite resolution) phase shifters. In practice, however, quantized PS are preferred thanks to the lower energy consumption and hardware complexity [42]–[44]. Quantized PS have a finite number of feasible phase shifts given by 2^{N_b}, where the number of quantization bits N_b are usually between 4 and 6 bits [45]. In order to adjust the proposed algorithm for the quantized PS case, we choose the closest quantized phases during the phase-extraction performed in lines 10 and 12 of Algorithm 1. In this experiment, we considered the same scenario as in the first experiment. Fig. 6 show the ratio between the sum-rate achieved by the non-quantized ($N_b = \infty$) and the quantized analog beamforming for SNR in the range $[-20, 10]$ dB. We observe that the quantized design can attain more than 99% of the non-quantized design's performance using $N_b = 6$ and more than 97% with $N_b = 5$ for the entire SNR range.

B. MMWAVE CHANNEL

Here, we present the results obtained for the mmWave channel. We assume a channel with $N_{cl} = 5$ and $N_{ray} = 10$, with average cluster power $\sigma^2_{\alpha,i} = 1$, angular spread $\sigma^t_\phi = \sigma^t_\theta = \sigma^r_\phi = \sigma^r_\theta = 10°$, and a USPA with antenna spacing $d = \lambda/2$. As for the Rayleigh channel, we start by evaluating the achievable sum-rate over different SNR values. We consider a 144×16 MU-MIMO with $K = 8$ users communicating through $N_s = 4$ data streams per user. The results in Fig. 7 show that the proposed method also outperformed all the other HBF designs in the mmWave configuration. The proposed design performs slightly better than the fully-digital design for low SNR (≤ -10 dB) and provides a performance improvement over the Hy-SBD that goes up to 6.3 bits/s/Hz at SNR $= -5$ dB.

Next, we evaluate the impact of the number of antennas on the achievable sum-rate. We consider a MU-MIMO system with $K = 4$ users having $N_r = 16$ receive antennas and communicating through $N_s = 4$ data streams at SNR $= -5$ dB. The results, depicted in Fig. 8, show that the proposed design can provide a fairly better sum-rate performance than the other designs when employing small

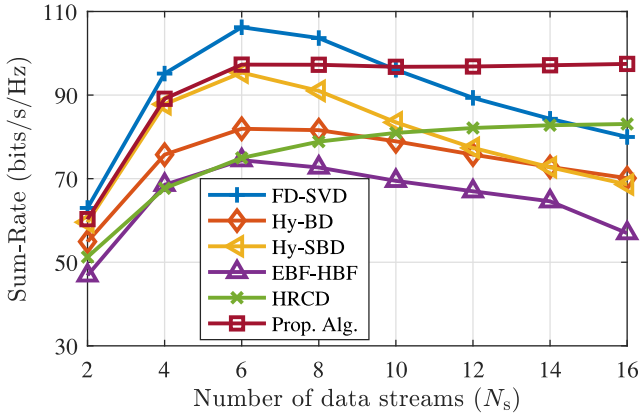

FIGURE 9. Sum-rate vs. number of data stream N_S for $N_t = 144$, $N_r = 16$, and $K = 4$ at SNR = 5 dB.

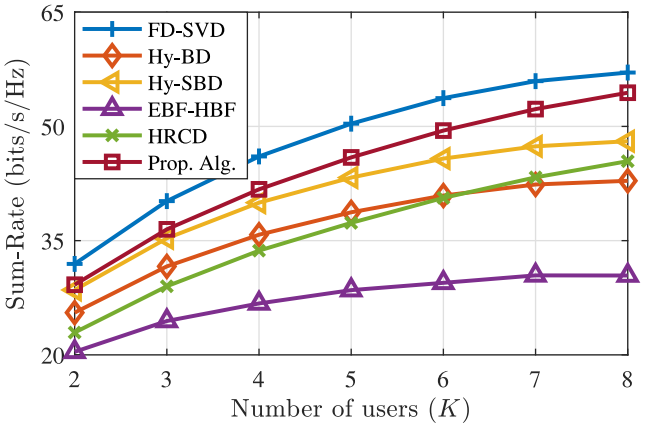

FIGURE 10. Sum-rate vs. number of users K for $N_t = 144$, $N_r = 16$, and $N_S = 4$ at SNR = -5 dB.

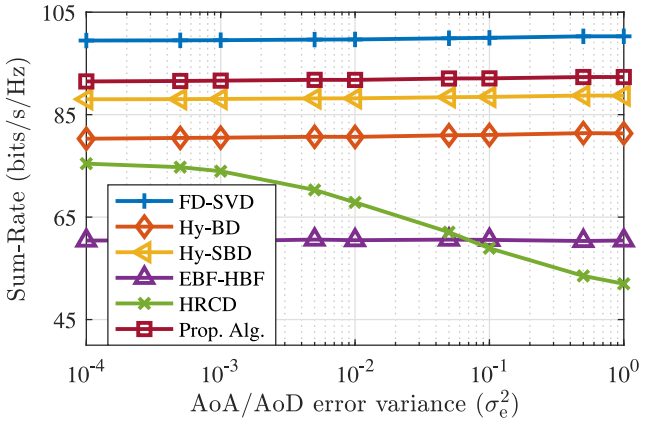

FIGURE 11. Sum-rate vs. angle estimation error variance for $N_t = 144$, $N_r = 16$, $K = 8$, and $N_S = 4$.

transmit arrays, attaining nearly 5.4 bits/s/Hz improvement over the Hy-SBD and 3.6 bits/s/Hz over the fully-digital design when $N_t = 25$.

In the following experiment, we assess the achievable sum-rate over different number of data streams N_s for a 144×16 MU-MIMO system with $K = 4$ users at SNR = 5 dB. The results are shown in Fig. 9, from which we can notice a significant improvement compared to the other designs. Such an improvement is largely thanks to the RCD digital precoding. Note that, except for the HRCD, which also adopts the RCD precoding, all the other designs, which employ traditional BD digital precoding, have their performance severely degraded as the number of data streams grows. The traditional BD transmits the signal of each user through the null-space of the other users and thus, by increasing the number of data streams, it reduces the dimension of the subspace each user can explore for transmission. In addition, note that this effect is much less present under Rayleigh channel in Fig. 4 thanks to its rich scattering environment. Here, in the most critical scenario ($N_s = 16$), the proposed design achieves sum-rate 14 bits/s/Hz and 28 bits/s/Hz higher than, respectively, the HRCD and the Hy-SBD.

The same reasoning is applied for the next experiment, where we evaluate the achieved sum-rate for different number of users K when considering a 144×16 MU-MIMO system communicating through $N_s = 4$ data stream at SNR $= -5$ dB. The results in Fig. 10 show that the HRCD and the proposed design preserve a growth trend as the number of users increases, while the other designs seem to stagnate. For $K = 8$, the proposed design exhibits more than 6.3 bits/s/Hz improvement over the Hy-SBD.

Next, we investigate the effect of channel estimation errors. HBF designs such as in [29], [32] require the knowledge of the AoAs and AoDs of all propagation paths. The angle estimation, however, is subjected to errors due to array imperfection, mutual coupling, gain/phase uncertainty and the positioning of the sensors [46], [47]. In order to evaluate the impact of imperfect channel estimation, we assume that the azimuth and elevation AoD ϕ_{il}^{t} and θ_{il}^{t} and AoA ϕ_{il}^{r} and θ_{il}^{r} are estimated with error. Since the phase error is usually much smaller then the support of the phase itself (e.g., 2π), we can assume it follows a Gaussian distribution with zero-mean and variance σ_e^2 [48]. Thus, in this experiment, we assess the sum-rate of a 144×16 MU-MIMO system with $K = 8$ users communicating through $N_s = 4$ data stream each at SNR $= 0$ dB. The results, depicted in Fig. 11, show the achieved sum-rate versus the AoA/AoD estimation error variance σ_e^2, with σ_e^2 ranging from 0.0001 ($\sigma_e \approx 0.57°$) to 1 ($\sigma_e \approx 57°$). Note that those designs that do not rely on the precise knowledge of the array response vector codebook have a fairly steady performance over the all the error variance range, while the HRCD, which rely on these codebooks, has its performance severely degraded, lowering nearly 25 bits/s/Hz of its error-free performance when $\sigma_e^2 = 1$.

Finally, we also evaluate the performance of the proposed design under quantized PS. Fig. 12 shows the ratio between the sum-rate achieved by the quantized and non-quantized PS scheme. The quantized design can attain more than 99.8% for $N_b = 6$, 99.5% for $N_b = 5$, and 98.3% for $N_b = 4$ over

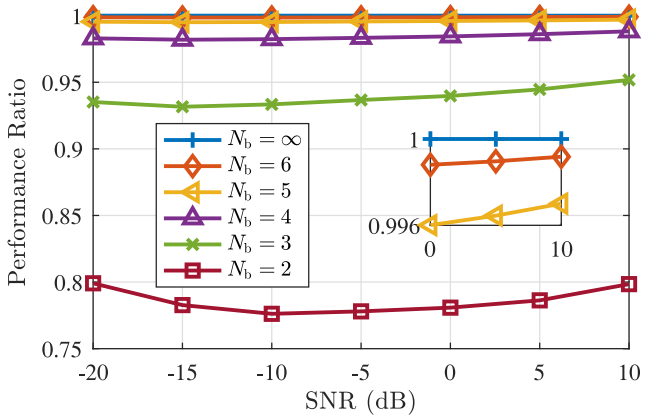

FIGURE 12. Ratio between sum-rate performance for quantized and non-quantized PS vs. the SNR for different number of quantization bits N_b.

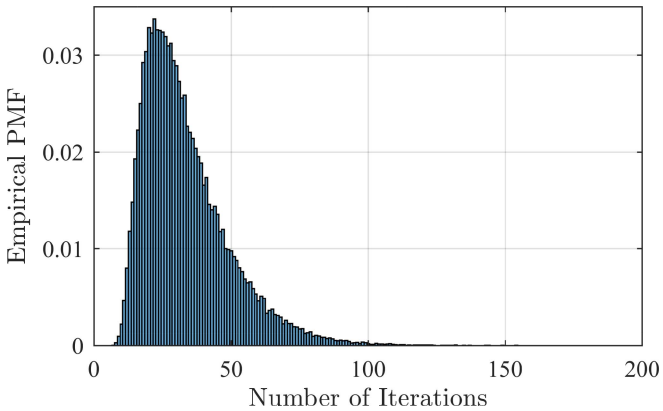

FIGURE 13. EPMF of the number of iterations for a 144 × 16 MU-MIMO with $K = 8$ users and $N_S = 4$ data streams per user in Rayleigh channel.

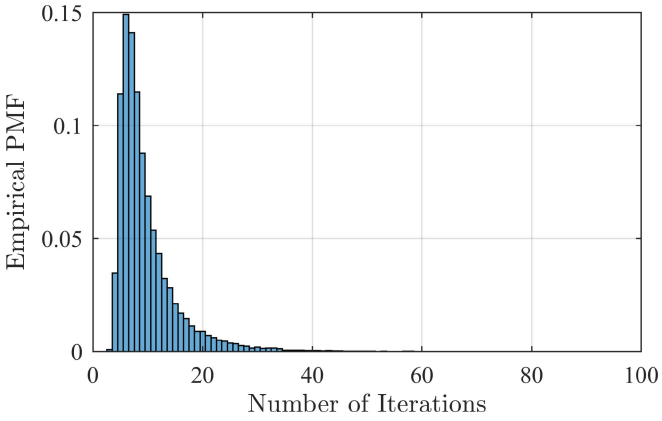

FIGURE 14. EPMF of the number of iterations for a 144 × 16 MU-MIMO with $K = 8$ users and $N_S = 4$ data streams per user in mmWave channel model.

all SNR range, indicating that the proposed scheme could be implemented with practical quantized PS with virtually no performance loss.

C. CONVERGENCE ANALYSIS

In order to evaluate the convergence of the proposed algorithm, we first recall the proof of optimality for the block coordinate problems related to (14), presented in the Appendix. Since the solutions in (16) are optimal, iterating between these solutions will lead to an increasingly better value for the cost function in (14). Therefore, the convergence is determined once the cost function ceases to increase. However, due to the non-convexity of (14), we cannot guarantee that this iterative process will converge to a global optimum solution, only to local ones.

Through extensive numerical simulations, we can gain important insights into the convergence of the proposed algorithm. Here, we evaluate the number of iterations required for the algorithm to converge. In Fig. 13 and Fig. 14 we present the empirical probability mass function (EPMF) of the number of iterations required to compute each analog precoder and combiner vector pair in a 144 × 16 MU-MIMO system with $K = 8$ and $N_s = 8$, respectively, for Rayleigh and mmWave channels. For the Rayleigh channel, Algorithm 1 required on average 33.4 iterations to find each analog precoder and combiner vector pair, and has converged with less than 84 iterations in more than 99% of the trials. For the mmWave channel, the algorithm required 9.6 iterations on average and has converged with less than 31 iterations in more than 99% of the cases. Nonetheless, we observe that the results in Figs. 13 and 14 remain fairly steady when varying system parameters, such as the number of antennas, users, or data streams; and have nearly the same shape when evaluated individually for each user or data stream. On the other hand, these results are highly dependent on the value of ε, the stopping criterion in Algorithm 1, allowing the designer to trade off performance for computational complexity.

The results also show that the proposed algorithm converges much faster in mmWave channels than in Rayleigh channels. Despite the lack of an analytical convergence proof (mainly due to the difficulty of handling the non-convexity of (14)), we infer that this phenomenon is associated with the fast decay of the channel' singular value energy, in contrast with the slowly decaying singular values in the Rayleigh channel, analogously to what happens for the unconstrained rank-1 approximation using the power iteration method [49]. Moreover, we observe that for mmWave channels, the algorithm is more likely to converge to the same (possibly the global optimal) solution, regardless of the initialization; while for Rayleigh channels, it may converge to different local optima, depending on the initialization.

D. FURTHER DISCUSSIONS

The results presented above have demonstrated that the proposed HBF design consistently outperforms the other design methods for both the rich scattering (Rayleigh fading) and limited scattering (mmWave) environments in a wide range of scenario parameters. In particular, the proposed design has shown significant improvement compared to other designs in the mmWave scenarios, as it has been seen in Figs. 9 and 10. Such an improvement is directly related to

the proposed design's ability to harvest the array gain and reduce the intra-user and multiuser interference in the analog beamforming stage, in contrast with other methods that only perform array gain harvesting, and the regularized digital precoder, which provides an important trade-off between MUI suppression and transmission diversity. Moreover, the results also revealed the capability of the proposed design to perform under practical constraints, such as the quantized-phase PS implementation of the analog beamforming and the imperfect channel state information.

V. CONCLUSION

In this article, we proposed a novel hybrid beamforming design for multiuser mmWave massive MIMO. The proposed method consists of a two-stage approach in which we design the analog and digital beamforming separately. The analog precoder and combiner design is based on a constrained low-rank channel approximation approach, which aims to harvest the array gain provided by the massive MIMO system while simultaneously reducing the MUI. The digital precoder and combiner are computed using the regularized channel diagonalization method, which trades off MUI suppression for more transmit diversity, thus attaining a better performance in low-SNR scenarios or when the number of users or data streams grows. In order to confirm the effectiveness of the proposed design, numerical simulation results have been provided for a wide range of scenarios. In addition, we evaluated the performance of our method under practical considerations, such as quantized PS and channel estimation errors. It has been shown that the proposed method outperforms the other HBF designs in all simulation scenarios.

APPENDIX
PROOF OF THE OPTIMALITY OF (16)

By adopting a different formulation to problem (14) and using the first and second order optimality conditions, we can demonstrate that the projected block coordinate solutions in (16) are, in fact, local optimal solutions to the non-convex block coordinate problems of (14). This result enables us to derive important insights on the convergence of the proposed algorithm. For conciseness, we omit the indices in the vectors and matrices and only present the solution to the block coordinate problem associated with the analog combiner vector. Such a problem is obtained from (14) as

$$\begin{aligned} \max_{\mathbf{w}} \quad & \mathrm{Re}\big(\mathbf{w}^{\mathrm{H}}\mathbf{H}_{\mathrm{res}}\mathbf{f}\big) \\ \text{s.t.} \quad & \|\mathbf{w}\| = 1 \\ & |[\mathbf{w}]_n| = 1/\sqrt{N_{\mathrm{r}}}, \ \forall n \in \{1,\ldots,N_{\mathrm{r}}\} \end{aligned} \tag{26}$$

We observe that: i) the second constraint in (26) guarantees that the first constraint be attained; and ii) using the second constraint, we can express the analog precoder vector as $\mathbf{w} = \frac{1}{\sqrt{N_{\mathrm{r}}}}[e^{j\theta_1}, e^{j\theta_2}, \ldots, e^{j\theta_{N_{\mathrm{r}}}}]^{\mathrm{T}} = \frac{1}{\sqrt{N_{\mathrm{r}}}}e^{j\boldsymbol{\theta}}$, with $\boldsymbol{\theta} = [\theta_1, \theta_2, \ldots, \theta_{N_{\mathrm{r}}}]^{\mathrm{T}}$. Thus, by defining $\mathbf{h} = [h_1, h_2, \ldots, h_{N_{\mathrm{r}}}]^{\mathrm{T}} = \mathbf{H}_{\mathrm{res}}\mathbf{f}$, with $h_i = |h_i|e^{j\phi_i}$, we can reformulate the cost function in (26) as

$$\begin{aligned} \mathcal{J} &= \mathrm{Re}\big\{\mathbf{w}^{\mathrm{H}}\mathbf{H}\mathbf{f}\big\} = \frac{1}{2}\big(\mathbf{w}^{\mathrm{H}}\mathbf{H}\mathbf{f} + \mathbf{f}^{\mathrm{H}}\mathbf{H}^{\mathrm{H}}\mathbf{w}\big) \\ &= \frac{1}{2\sqrt{N_{\mathrm{r}}}}\left(\sum_{i=1}^{N_{\mathrm{r}}} e^{-j\theta_i}h_i + \sum_{i=1}^{N} e^{j\theta_i}h_i^*\right) \\ &= \frac{1}{2\sqrt{N_{\mathrm{r}}}}\sum_{i=1}^{N_{\mathrm{r}}}|h_i|\Big(e^{-j(\theta_i-\phi_i)} + e^{j(\theta_i-\phi_i)}\Big) \\ &= \frac{1}{\sqrt{N_{\mathrm{r}}}}\sum_{i=1}^{N_{\mathrm{r}}}|h_i|\mathrm{Re}\Big\{e^{-j(\theta_i-\phi_i)}\Big\} \end{aligned} \tag{27}$$

Thus, the optimization problem in (26) is equivalent to the following unconstrained optimization problem

$$\arg\max_{\boldsymbol{\theta}\in\mathbb{R}^{N_{\mathrm{r}}}} \quad \sum_{i=1}^{N_{\mathrm{r}}}|h_i|\mathrm{Re}\{e^{-j(\theta_i-\phi_i)}\}. \tag{28}$$

The solution to problem (28) is obtained using the first- and second-order optimality conditions [50], i.e.,

$$\nabla_{\boldsymbol{\theta}}\mathcal{J} = \frac{1}{\sqrt{N_{\mathrm{r}}}}\begin{bmatrix} |h_1|\mathrm{Re}\{e^{-j(\theta_1-\phi_1+\pi/2)}\} \\ |h_2|\mathrm{Re}\{e^{-j(\theta_2-\phi_2+\pi/2)}\} \\ \vdots \\ |h_{N_{\mathrm{r}}}|\mathrm{Re}\{e^{-j(\theta_{N_{\mathrm{r}}}-\phi_{N_{\mathrm{r}}}+\pi/2)}\} \end{bmatrix} = \mathbf{0} \tag{29}$$

and

$$\nabla^2_{\boldsymbol{\theta}}\mathcal{J} = \frac{1}{\sqrt{N_{\mathrm{r}}}}\mathrm{diag}\left(\begin{bmatrix} |h_1|\mathrm{Re}\Big\{e^{-j(\theta_1-\phi_1+\pi)}\Big\} \\ |h_2|\mathrm{Re}\Big\{e^{-j(\theta_2-\phi_2+\pi)}\Big\} \\ \vdots \\ |h_{N_{\mathrm{r}}}|\mathrm{Re}\Big\{e^{-j(\theta_{N_{\mathrm{r}}}-\phi_{N_{\mathrm{r}}}+\pi)}\Big\} \end{bmatrix}\right) \prec \mathbf{0} \tag{30}$$

where $\mathrm{diag}(\mathbf{v})$ is a diagonal matrix with diagonal entries given by $\mathbf{v}$ and $\mathbf{A} \prec 0$ when $\mathbf{A}$ is negative-definite. Together, these conditions yield multiple local optimal solutions, given as

$$\theta_i = \phi_i \pm 2\pi k, \quad \text{for } k = 0, 1, 2, \ldots, \tag{31}$$

Thus, if we choose the trivial solution ($k = 0$), we obtain $\theta_i = \phi_i$, so that an optimal solution to problem (28) is given by

$$\boldsymbol{\theta} = \boldsymbol{\phi} = \angle\{\mathbf{H}\mathbf{f}\} \tag{32}$$

or equivalently, an optimal solution to problem (26) is given by

$$\mathbf{w} = \frac{1}{\sqrt{N_{\mathrm{r}}}}e^{j\boldsymbol{\phi}} = \frac{1}{\sqrt{N_{\mathrm{r}}}}e^{j\angle\mathbf{H}_{\mathrm{res}}\mathbf{f}}. \tag{33}$$

ACKNOWLEDGMENT

The authors are thankful to the Editor and anonymous reviewers for insightful comments that greatly improved the manuscript. They are also thankful to Dr. Rui Seara for providing access to high-performance computing resources at the LINSE – Circuit and Signal Processing Laboratory of the Federal University of Santa Catarina, Brazil.

REFERENCES

[1] Z. Zhang *et al.*, "6G wireless networks: Vision, requirements, architecture, and key technologies," *IEEE Veh. Technol. Mag.*, vol. 14, no. 3, pp. 28–41, Sep. 2019.

[2] K. Samdanis and T. Taleb, "The road beyond 5G: A vision and insight of the key technologies," *IEEE Netw.*, vol. 34, no. 2, pp. 135–141, Mar./Apr. 2020.

[3] M. Giordani, M. Polese, M. Mezzavilla, S. Rangan, and M. Zorzi, "Toward 6G networks: Use cases and technologies," *IEEE Commun. Mag.*, vol. 58, no. 3, pp. 55–61, Mar. 2020.

[4] M. Z. Chowdhury, M. Shahjalal, S. Ahmed, and Y. M. Jang, "6G wireless communication systems: Applications, requirements, technologies, challenges, and research directions," *IEEE Open J. Commun. Soc.*, vol. 1, pp. 957–975, 2020.

[5] L. Wei, R. Q. Hu, Y. Qian, and G. Wu, "Key elements to enable millimeter wave communications for 5G wireless systems," *IEEE Wireless Commun.*, vol. 21, no. 6, pp. 136–143, Dec. 2014.

[6] J. G. Andrews *et al.*, "What will 5G be?" *IEEE J. Sel. Areas Commun.*, vol. 32, no. 6, pp. 1065–1082, Jun. 2014.

[7] Q. Bi, "Ten trends in the cellular industry and an outlook on 6G," *IEEE Commun. Mag.*, vol. 57, no. 12, pp. 31–36, Dec. 2019.

[8] Z. Pi and F. Khan, "An introduction to millimeter-wave mobile broadband systems," *IEEE Commun. Mag.*, vol. 49, no. 6, pp. 101–107, Jun. 2011.

[9] T. S. Rappaport *et al.*, "Millimeter wave mobile communications for 5G cellular: It will work!" *IEEE Access*, vol. 1, pp. 335–349, 2013.

[10] A. A. Nasir, H. D. Tuan, T. Q. Duong, H. V. Poor, and L. Hanzo, "Hybrid beamforming for multi-user millimeter-wave networks," *IEEE Trans. Veh. Technol.*, vol. 69, no. 3, pp. 2943–2956, Mar. 2020.

[11] R. W. Heath, N. Gonzalez-Prelcic, S. Rangan, W. Roh, and A. M. Sayeed, "An overview of signal processing techniques for millimeter wave MIMO systems," *IEEE J. Sel. Topics Signal Process.*, vol. 10, no. 3, pp. 436–453, Apr. 2016.

[12] J. Zhang, X. Yu, and K. B. Letaief, "Hybrid beamforming for 5G and beyond millimeter-wave systems: A holistic view," *IEEE Open J. Commun. Soc.*, vol. 1, pp. 77–91, 2020.

[13] M. Rihan, T. A. Soliman, C. Xu, L. Huang, and M. I. Dessouky, "Taxonomy and performance evaluation of hybrid beamforming for 5G and beyond systems," *IEEE Access*, vol. 8, pp. 74605–74626, 2020.

[14] I. Ahmed *et al.*, "A survey on hybrid beamforming techniques in 5G: Architecture and system model perspectives," *IEEE Commun. Surveys Tuts.*, vol. 20, no. 4, pp. 3060–3097, 4th Quart., 2018.

[15] A. Alkhateeb, J. Mo, N. Gonzalez-Prelcic, and R. W. Heath, "MIMO precoding and combining solutions for millimeter-wave systems," *IEEE Commun. Mag.*, vol. 52, no. 12, pp. 122–131, Dec. 2014.

[16] A. F. Molisch *et al.*, "Hybrid beamforming for massive MIMO: A survey," *IEEE Commun. Mag.*, vol. 55, no. 9, pp. 134–141, Sep. 2017.

[17] O. El Ayach, S. Rajagopal, S. Abu-Surra, Z. Pi, and R. W. Heath, "Spatially sparse precoding in millimeter wave MIMO systems," *IEEE Trans. Wireless Commun.*, vol. 13, no. 3, pp. 1499–1513, Mar. 2014.

[18] X. Yu, J.-C. Shen, J. Zhang, and K. B. Letaief, "Alternating minimization algorithms for hybrid precoding in millimeter wave MIMO systems," *IEEE J. Sel. Topics Signal Process.*, vol. 10, no. 3, pp. 485–500, Apr. 2016.

[19] F. Sohrabi and W. Yu, "Hybrid digital and analog beamforming design for large-scale antenna arrays," *IEEE J. Sel. Topics Signal Process.*, vol. 10, no. 3, pp. 501–513, Apr. 2016.

[20] D. Zhang, P. Pan, R. You, and H. Wang, "SVD-based low-complexity hybrid precoding for millimeter-wave MIMO systems," *IEEE Commun. Lett.*, vol. 22, no. 10, pp. 2176–2179, Oct. 2018.

[21] G. M. Zilli and W.-P. Zhu, "Constrained-SVD based hybrid beamforming design for millimeter wave communications," in *Proc. IEEE 92nd Veh. Technol. Conf. (VTC-Fall)*, Victoria, BC, Canada, Oct. 2020, pp. 1–5.

[22] L. Liang, W. Xu, and X. Dong, "Low-complexity hybrid precoding in massive multiuser MIMO systems," *IEEE Wireless Commun. Lett.*, vol. 3, no. 6, pp. 653–656, Dec. 2014.

[23] J. Li, L. Xiao, X. Xu, and S. Zhou, "Robust and low complexity hybrid beamforming for uplink multiuser mmWave MIMO systems," *IEEE Commun. Lett.*, vol. 20, no. 6, pp. 1140–1143, Jun. 2016.

[24] A. Alkhateeb, R. W. Heath, and G. Leus, "Achievable rates of multi-user millimeter wave systems with hybrid precoding," in *Proc. IEEE Int. Conf. Commun. Workshop*, London, U.K., Jun. 2015, pp. 1232–1237.

[25] A. Alkhateeb, G. Leus, and R. W. Heath, "Limited feedback hybrid precoding for multi-user millimeter wave systems," *IEEE Trans. Wireless Commun.*, vol. 14, no. 11, pp. 6481–6494, Nov. 2015.

[26] A. Li and C. Masouros, "Hybrid precoding and combining design for millimeter-wave multi-user MIMO based on SVD," in *Proc. IEEE Int. Conf. Commun.*, Paris, France, May 2017, pp. 1–6.

[27] Z. Wang, M. Li, X. Tian, and Q. Liu, "Iterative hybrid precoder and combiner design for mmWave multiuser MIMO systems," *IEEE Commun. Lett.*, vol. 21, no. 7, pp. 1581–1584, Jul. 2017.

[28] W. Ni and X. Dong, "Hybrid block diagonalization for massive multiuser MIMO systems," *IEEE Trans. Commun.*, vol. 64, no. 1, pp. 201–211, Jan. 2016.

[29] R. Rajashekar and L. Hanzo, "Iterative matrix decomposition aided block diagonalization for mm-wave multiuser MIMO systems," *IEEE Trans. Wireless Commun.*, vol. 16, no. 3, pp. 1372–1384, Mar. 2017.

[30] X. Wu, D. Liu, and F. Yin, "Hybrid beamforming for multi-user massive MIMO systems," *IEEE Trans. Commun.*, vol. 66, no. 9, pp. 3879–3891, Sep. 2018.

[31] C. Hu, J. Liu, X. Liao, Y. Liu, and J. Wang, "A novel equivalent baseband channel of hybrid beamforming in massive multiuser MIMO systems," *IEEE Commun. Lett.*, vol. 22, no. 4, pp. 764–767, Apr. 2018.

[32] F. Khalid, "Hybrid beamforming for millimeter wave massive multiuser MIMO systems using regularized channel diagonalization," *IEEE Wireless Commun. Lett.*, vol. 8, no. 3, pp. 705–708, Jun. 2019.

[33] Q. H. Spencer, A. L. Swindlehurst, and M. Haardt, "Zero-forcing methods for downlink spatial multiplexing in multiuser MIMO channels," *IEEE Trans. Signal Process.*, vol. 52, no. 2, pp. 461–471, Feb. 2004.

[34] X. Cheng, C. Tang, and Z. Zhang, "Accurate channel estimation for millimeter-wave MIMO systems," *IEEE Trans. Veh. Technol.*, vol. 68, no. 5, pp. 5159–5163, May 2019.

[35] E. Vlachos, G. C. Alexandropoulos, and J. Thompson, "Wideband MIMO channel estimation for hybrid beamforming millimeter wave systems via random spatial sampling," *IEEE J. Sel. Topics Signal Process.*, vol. 13, no. 5, pp. 1136–1150, Sep. 2019.

[36] T. G. Kolda, "Multilinear operators for higher-order decompositions," Sandia Nat. Lab., Albuquerque, NM, USA, Rep. SAND2006-2081, 2006.

[37] T. G. Kolda and B. W. Bader, "Tensor decompositions and applications," *SIAM Rev.*, vol. 51, no. 3, pp. 455–500, Aug. 2009.

[38] H.-J. M. Shi, S. Tu, Y. Xu, and W. Yin, "A primer on coordinate descent algorithms," Jan. 2017. [Online]. Available: https://arxiv.org/abs/1610.00040.

[39] Y. Chi, Y. M. Lu, and Y. Chen, "Nonconvex optimization meets low-rank matrix factorization: An overview," *IEEE Trans. Signal Process.*, vol. 67 no. 20, pp. 5239–5269, Oct. 2019.

[40] V. Stankovic and M. Haardt, "Generalized design of multi-user MIMO precoding matrices," *IEEE Trans. Wireless Commun.*, vol. 7, no. 3, pp. 953–961, Mar. 2008.

[41] F. Khalid and J. Speidel, "Robust hybrid precoding for multiuser MIMO wireless communication systems," *IEEE Trans. Wireless Commun.*, vol. 13, no. 6, pp. 3353–3363, Jun. 2014.

[42] J.-C. Chen, "Hybrid beamforming with discrete phase shifters for millimeter-wave massive MIMO systems," *IEEE Trans. Veh. Technol.*, vol. 66, no. 8, pp. 7604–7608, Aug. 2017.

[43] Z. Wang, M. Li, Q. Liu, and A. L. Swindlehurst, "Hybrid precoder and combiner design with low-resolution phase shifters in mmWave MIMO systems," *IEEE J. Sel. Topics Signal Process.*, vol. 12, no. 2, pp. 256–269, May 2018.

[44] F. Dong, W. Wang, and Z. Wei, "Low-complexity hybrid precoding for multi-user mmWave systems with low-resolution phase shifters," *IEEE Trans. Veh. Technol.*, vol. 68, no. 10, pp. 9774–9784, Oct. 2019.

[45] *RF, Microwave, and Millimeter Wave Products: Selection Guide*, Analog Devices, Norwood, MA, USA, 2020. Accessed: Jul. 20, 2020. [Online]. Available: https://www.analog.com/en/products/rf-microwave.html

[46] Z.-M. Liu, "Conditional Cramér–Rao lower bounds for DOA estimation and array calibration," *IEEE Signal Process. Lett.*, vol. 21, no. 3, pp. 361–364, Mar. 2014.

[47] H. Huang, M. Faus, and A. M. Zoubir, "Block sparsity-based DOA estimation with sensor gain and phase uncertainties," in *Proc. 27th Eur. Signal Process. Conf. (EUSIPCO)*, A Coruna, Spain, Sep. 2019, pp. 1–5.

[48] M.-C. Yue, S. X. Wu, and A. M.-C. So, "A robust design for MISO physical-layer multicasting over line-of-sight channels," *IEEE Signal Process. Lett.*, vol. 23, no. 7, pp. 939–943, Jul. 2016.
[49] G. H. Golub and C. F. Van Loan, *Matrix Computations*, 4th ed. Baltimore, MD, USA: Johns Hopkins Univ. Press, 2013.
[50] D. G. Luenberger and Y. Ye, *Linear and Nonlinear Programming*, 3rd ed. New York, NY, USA: Springer, 2008.

GUILHERME MARTIGNAGO ZILLI (Graduate Student Member, IEEE) received the B.S. degree in electrical engineering from Santa Catarina State University, Joinville, Brazil, in 2014, and the M.Sc. degree in electrical engineering from the Federal University of Santa Catarina, Florianópolis, Brazil, in 2016. He is currently pursuing the Ph.D. degree in electrical engineering with Concordia University, Montreal, QC, Canada.

His research interests include signal processing and wireless communications, with emphasis on beamforming design. He is a recipient of the Doctoral Research Scholarship Program for Foreign Students, from the Fonds de recherche du Québec—Nature et Technologies (FRQNT) and the Concordia International Tuition Award of Excellence.

WEI-PING ZHU (Senior Member, IEEE) received the B.E. and M.E. degrees in electrical engineering from the Nanjing University of Posts and Telecommunications in 1982 and 1985, respectively, and the Ph.D. degree in electrical engineering from Southeast University, Nanjing, China, in 1991.

He was a Postdoctoral Fellow from 1991 to 1992, and a Research Associate from 1996 to 1998, with the Department of Electrical and Computer Engineering, Concordia University, Montreal, Canada. From 1993 to 1996, he was an Associate Professor with the Department of Information Engineering, Nanjing University of Posts and Telecommunications. From 1998 to 2001, he worked with hi-tech companies in Ottawa, Canada, including Nortel Networks and SR Telecom, Inc. Since July 2001, he has been with Concordia's Electrical and Computer Engineering Department as a full-time Faculty Member, where he is currently a Full Professor. His research interests include digital signal processing fundamentals, speech and statistical signal processing, and signal processing for wireless communication with a particular focus on MIMO systems and cooperative communication. He was the Secretary of Digital Signal Processing Technical Committee (DSPTC) of the IEEE Circuits and System Society from June 2012 to May 2014, and the Chair of the DSPTC from June 2014 to May 2016. He was also a Guest Editor for the IEEE JOURNAL ON SELECTED AREAS IN COMMUNICATIONS for the special issues of: Broadband Wireless Communications for High Speed Vehicles, and Virtual MIMO from 2011 to 2013. He was served as an Associate Editor for the IEEE TRANSACTIONS ON CIRCUITS AND SYSTEMS PART I: FUNDAMENTAL THEORY AND APPLICATIONS from 2001 to 2003, an Associate Editor for *Circuits, Systems, and Signal Processing* from 2006 to 2009, and an Associate Editor for the IEEE TRANSACTIONS ON CIRCUITS AND SYSTEMS II: EXPRESS BRIEFS, from 2011 to 2015. He is an Associate Editor of *Journal of the Franklin Institute*.